FC

Technical Report

To The

Office of Naval Research

On

THE ANODIC BEHAVIOR OF IRON

by

Norman Hackerman and William H. Wade

July 15, 1955

Contract Nonr - 375(02)

Department of Chemistry
The University of Texas

Austin, Texas

SYMBOLS

V	volts
A	amperes
mA	milliamperes
uA	microamperes
uC	microcoulombs
$T.cm.^2$	square centimeters of true area
$A.cm.^2$	square centimeters of apparent area
a, a'	Tafel curve intercepts
b	Tafel curve slope
δ	Thickness of the diffusion layer
ν	stoichiometric number
E_m	measured oxygen evolution potential
E_r	resistance overvoltage
E_c	concentration overvoltage
E_a	activation overvoltage
E_o	overvoltage
pH_c	change in pH due to concentration overvoltage
pH_b	bulk pH
R	$E_r/A/T.cm.^2$ for resistance overvoltage decay

SUMMARY

The anodic behavior of pure iron electrodes was studied in
0.1 M Na_2SO_4 at 5° C. Oxygen overvoltage measurements in acid
solutions showed the mechanism to be the oxidation of water mole-
cules to adsorbed hydroxyl radicals, next, the dehydration of
two of these radicals to give an adsorbed oxygen atom, followed
by the desorptive combination of two of these oxygen atoms. Oxy-
gen overvoltage-time decay measurements for these solutions in-
dicate that there is little possibility of other chemical spe-
cies being present on the passive iron surface. The primary cov-
erage is postulated as adsorbed hydroxyl radicals in conformance
with the slow step in the oxygen evolution mechanism. As it is,
the coverage is only 10 percent with respect to iron atoms in the
surface. The surface coverage, as measured by the decay curves
was found to fall off at oxygen evolution current densities of
less than 0.5 uA/T.cm.^{2} This would be predicted on the basis of
a purely chemical path for the removal of the adsorbed hydroxyl
radicals, namely, the last two steps of the oxygen evolution me-
chanism.

In alkaline solutions, overvoltage measurements and potential-
time decay curves both led to the conclusion that the passive
iron surface is primarily covered with adsorbed hydroxyl ions.
The mechanism of oxygen evolution differs from that for the acid
solutions. It is the oxidation of adsorbed hydroxyl ions to hy-
droxyl radicals, next, the dehydration of two hydroxyl radicals
to give an adsorbed oxygen atom, followed by reaction of this oxy-
gen atom with an adsorbed hydroxyl ion to form a desorbed oxygen
molecule. Once again, the coverage was found to be only 10 percent

INTRODUCTION

On anodic polarization active metals are oxidized, whereas,
with inert metal electrodes the reacting species must come from
a source other than the metal itself. Platinum, for example, suf-
fers little or no chemical attack on anodic polarization, except
in high chloride ion concentrations. Working with large cur-
rents, Bowden[1] found that shifting the potential of platinum
from hydrogen evolution ot oxygen evolution required about 3000
microcoulombs/cm.^{2} In addition there were potential arrests
corresponding to adsorbed hydrogen and its replacement by adsor-
bed oxygen. Butler and Armstrong[2] studied this same system and
found that upon cathodic polarization of a platinum electrode
previously anodically polarized in dilute H_2SO_4, there was a po-
tential arrest in the region of +0.7 volt (relative to the hy-
drogen electrode). While at this potential both adsorbed oxygen
and oxygen dissolved in solution were assumed to be reduced.
Only 200 uC/T.cm.^{2} were required for reduction of the adsorbed
oxygen. Bowden suggests that the surface layer is not adsorbed
oxygen but a monolayer of platinum oxide. Ershler[3] studied
the anodic dissolution of platinum in chloride solutions and
found a marked decrease in the corrosion rate of the platinum
when the surface is only 6 to 7 per cent covered with

oxygen. This he attributes to the repulsion of chloride ions by the negative space charge set up by the adsorbed oxygen.

Other inert metals, such as gold[2] and some of the metals of the platinum group[4], show the same general behavior on anodic polarization. On cathodic polarization of anodically polarized gold electrodes, there are two potential arrests: the first corresponding to the removal of an auric oxide, and the second to the removal of adsorbed oxygen. Some of the other metals of the platinum group form visible oxides on anodic polarization, but subsequent cathodic polarization always gives a potential arrest corresponding to the reduction of adsorbed oxygen. These methods of determining surface concentrations are very sensitive, the determination of 10^{-11} equivalent of oxide or 10^{14} atoms of oxygen being easily possible.

There is the possibility of oxygen evolution becoming the predominant anodic reaction at the surface of an apparently active metal upon meeting certain conditions, i.e., the metal is said to be passive. For example, if iron is polarized anodically at a sufficient current density, in the proper electrolyte solution, first there is dissolution of iron which suddenly stops and simultaneously oxygen evolution begins. During the transition between these two reactions, the electrode potential falls rapidly from a value compatible with the dissolution of iron to a value exceeding that predicted for the reversible oxygen electrode. This potential drop usually amounts to more than one volt. Normally, it would be expected that oxygen evolution could occur simultaneously with iron dissolution if the current density was raised sufficiently to shift the electrode potential to a value indicative of oxygen evolution. These high currents are attained from a physical masking of the electrode surface by precipitation of ferrous salts, which in effect block most of the surface. This greatly increases the current density for the remaining exposed surface. This mechanism has been extensively studied by Mueller, and his work is summarized by Evans.[5]

A difficulty arises in the explanation of the complete cessation of the dissolution of the iron. It is widely believed that when oxygen evolution commences, a protective covering has been formed on the surface. It is the nature of this covering that causes most of the controversy in the field of passivity.

Active metals which can evolve oxygen behave in one of two ways when they are treated anodically. Aluminum, lead, zinc, titanium, and some other metals form visible oxides which adhere to the metal surface. Iron, chromium, nickel, and several other metals do not form visible coatings, even over long periods of such treatment.

In both cases, Evans[6] considers passivity to be due to

the formation of an oxide film on the surface of the metal, the oxide remaining invisibly thin for the iron group of metals. Although a very thin and almost transparent film of Fe_2O_3 was successfully stripped from the surface of passive iron, there is no evidence that this oxide film actually existed on the surface of the iron. Nevertheless, Evans considers that a layer of Fe_2O_3 forms a physical barrier isolating the metal surface from a potentially corrosive environment. This is the generally accepted theory.

Bonhoeffer[7], upon introducing cathodic pulses to an iron electrode passivated in concentrated HNO_3, concluded that the surface was covered with a monolayer of Fe_2O_3. He found that 200 uC/A.cm.[2] were required to break this monolayer down. Roberts and Shut[8] carried out the same type of determination on chromium, and concluded that the passive chromium surface is covered with Cr_2O_3 to the extent of a monolayer. There was some uncertainty because of the difficulty in measuring the true surface area of the electrodes. From the number of coulombs passed in the passivation of nickel, cobalt, and copper, Hickling[9] considers the passive covering to consist of a monolayer of the respective oxides. If all these monolayer quantities are valid, then these oxide layers would not be visible, much less stable, if they were stripped from the surface of the metal.

Other theories of passivity concede that metals such as aluminum are protected by a thick oxide layer and discuss the passivation layer of the other group of metals on a different basis. Fontana and Beck[10] concluded that physically adsorbed gases are important to the passivation of stainless steels. They were able to activate steel samples, made passive in H_2SO_4, by evacuation of the system.

Uhlig[11] developed the electron configuration theory which he first applied to the iron-chromium alloys. He states that chromium is naturally passive due to an incomplete 3d shell, and is able to impart passivity to iron on alloying the two metals. The assumption is that chromium, having 5, 3d electrons, can accept 5 electrons from the alloyed iron atoms -- one electron from each iron atom -- to produce a completed 3d shell. Thus an alloy containing 16 mole per cent of chromium should be naturally passive. This is in agreement with observed properties of these alloys, and the method has been extended with equal success to other alloy systems. There seem to be several obstacles to the acceptance of this theory. Chromium is not naturally passive, it is easily passivated. If the iron is passivated by the removal of its d electrons, why is not the chromium activated by the acceptance of these electrons? Besides this, Heumann[12] has pointed out that the electron configurations used by Uhlig were for the gaseous state and are not valid from the consideration

of the band structure of metals. Heumann also points out
that most electron transferrences would be in the opposite
direction.

Uhlig has extended the concepts of the electron trans-
fer into a generalized film theory[13], which has much merit
in that there is a realization of the important aspect of
specific interaction between the passivating layer and the
underlying metal. In the generalized film theory the passi-
vating layer is chemisorbed and removes electrons from the
metal surface to form a polarized bond. Thus, chemisorption
serves the same purpose as alloying with chromium. From this
viewpoint, a multitude of substances could passivate a metal's
surface. Likewise, the activating action of adsorbed and
absorbed hydrogen can be explained by donation of electrons
to the metal with formation of H^+ ions.

Assuming the validity of the generalized film theory,
a passive surface evolving oxygen might be covered with
chemisorbed oxygen atoms. Experiments on the adsorption of
oxygen from the gas phase onto the surface of these metals
indicate that the bonds formed are very strong and polarized
so that the oxygen atoms are negative with respect to the
surface of the metal. Weisz[14] has derived an equation showing
that only a small fraction of the surface need be covered
to obtain a uniform negative space charge density, and that
in many cases of chemisorption with polarization of the
bonds, it is impossible to completely cover the surface.

Despite the effort that has gone into deducing the na-
ture of this passive film, there is still a need for a criti-
cal experiment to examine the film in situ. The present
work may furnish some insight into the nature of this cover-
ing on passive iron, as well as information on its associated
anodic behavior.

Experimental Apparatus and Chemicals

Chemicals.

The iron used in all experiments was supplied by the
Armco Steel Corporation. Their analysis showed the follow-
ing impurities: C, 0.010; Mn, 0.010; P, 0.005; Si, 0.002;
Cu, 0.040%.

Grade A helium obtained from the Amarillo Division of
the Bureau of Mines was bubbled through the solutions. Their
assay shows it to be 99,997 per cent pure, with less than
10^{-6} per cent of either oxygen or water vapor.

All solutions used were 0.1 M in Na_2SO_4. These solutions
were prepared by taking aliquots from a single bottle of 1.0
M Na_2SO_4, made with distilled water and C.P. Na_2SO_4. The
pH of the solutions was varied by addition of C.P. H_2SO_4 or
C.P. NaOH. Buffers were not used to stabilize the pH of any

of the solutions. All water used for preparing the solutions was distilled "equilibrium" water.
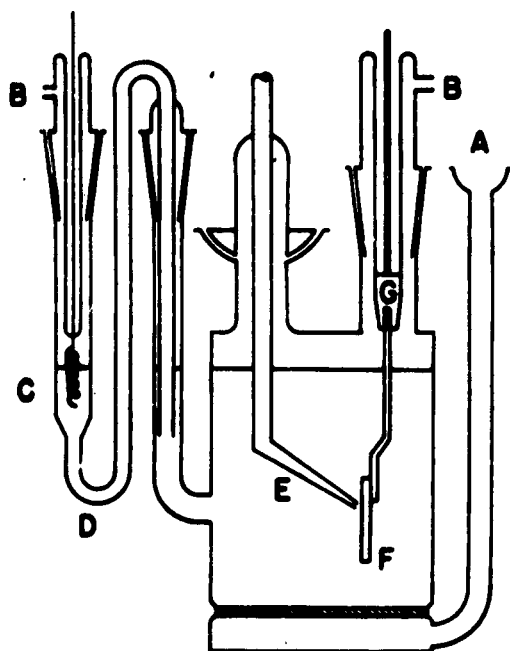
Coupons

All coupons were cut from the same sheet, and measured approximately 2 x 3 cm. Steel rods, spot welded to the coupons, were used as electrical contact and support for the coupons. The coupons were annealed at 1000° C. in a vacuum of 10^{-6} mm.Hg. for 1/2 hour. Mercury vapor was kept from the annealing oven by the use of two dry-ice-isopropanol cold traps. Prior to each experiment, the coupons were polished with number 2 emery paper and degreased in benzene. The exposed area of the electrode was formed by Willbanks'[15] method. A celluloid washer was placed on the electrode, and Ucilon was introduced between the washer and the surface of the electrode. Except for the exposed surface in the center of the washer, all the remainder of the coupon was covered with Myvawax. This gave a reproducible area of 0.24 ± 0.02 cm.[2] Myvawax was chosen to mask the electrode for, unlike paraffin, it does not have the tendency to crack at the temperatures used in this work. The apparent area was determined at the end of each run with a traveling microscope. The diameter of the circular spot formed on the coupon was measured from four different positions and the average of the four used to calculate the apparent area.

Polarization Cell.

The design of the polarization cell is shown approximately 1/2 size in Figure 1a. The steel rods with attached coupons screw into the holder (G). The holder consisted of a Kovar glass to metal seal with an inserted brass plug tapped to receive the steel rod. The auxiliary polarizing electrode was made of platinum wire sealed into Pyrex. The possibility of diffusion of dissolved hydrogen from the auxiliary electrode to the iron electrode was eliminated by the use of solution bridge (D). Likewise, solution contact between the reference electrode and the iron coupon was effected by means of a bridge containing the experimental solution. This bridge, (E), prevented chloride ions from the reference electrode diffusing to the experimental electrode. A saturated calomel electrode (potential relative to the hydrogen electrode of +0.259v.) was used as the reference. Unless otherwise stated potentials are relative to this electrode. The solution bridge for the reference electrode terminated in a capillary tip which, by manipulation of the ball joint, could be placed close to the surface of the electrode. Stirring was accomplished by bubbling helium through the solution, the inlet being at (A). The outlets for helium and any gases evolved at the electrodes are (B). For all experiments, the cell was immersed in a constant temperature water bath thermostatted to $5 \pm 0.2°$ C.

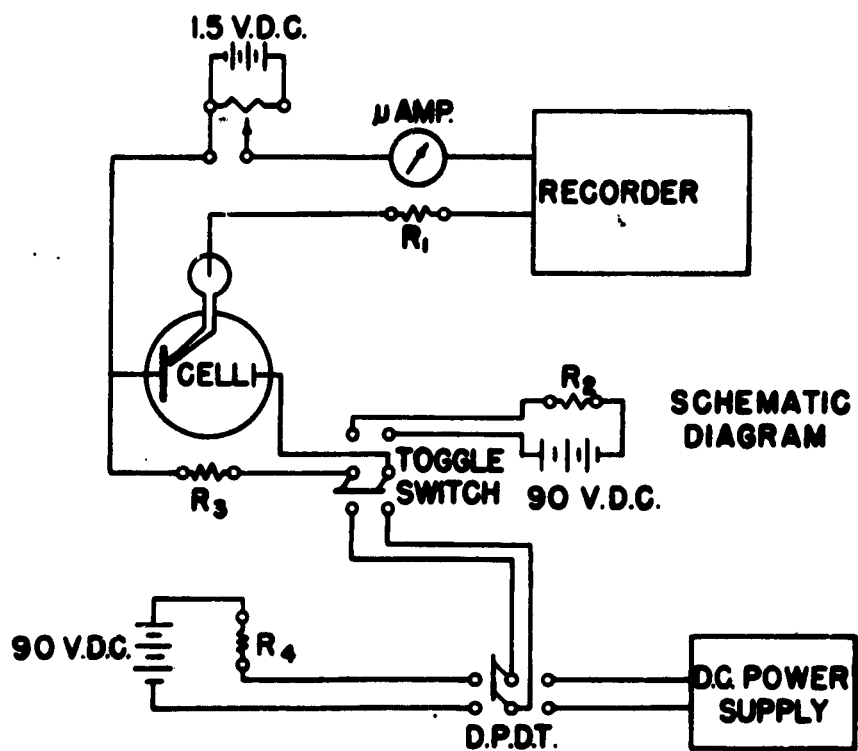Figure 1A. The experimental cell.

Figure 1B. The schematic diagram of the
electrical circuit.

POLARIZATION CELL

A.

1.5 V.D.C.

μ AMP.

RECORDER

R_1

CELL

R_2

SCHEMATIC DIAGRAM

TOGGLE SWITCH

90 V.D.C.

R_3

90 V.D.C.

R_4

D.P.D.T.

D.C. POWER SUPPLY

B.

Electrical Circuit.

A schematic diagram of the polarizing and measuring circuit is shown in Figure 1B. Anodic polarization currents were supplied either by a D.C. power supply or a 90 volt battery. The D.C. power supply produced the relatively large currents needed to passivate the coupons. When the coupons were passivated, the smaller currents necessary to maintain the passive state were drawn from the 90 volt source. Cathodic polarization currents were taken from another 90 volt battery. Measurements indicated that currents were constant to 0.1 per cent over a 2 hour period. The electrical leads for both the anodic and cathodic sources terminated in a toggle switch so that it was possible to change rapidly from anodic to cathodic polarization. The current density was varied by interchange of series resistors in the polarizing circuits. The exact value of the current was determined by measurement of the voltage drop across a precision resistor.

Time-potential traces were taken with an automatic recording potentiometer, a model V153X(19)(V)-X-66 Minneappolis Honeywell, Brown Electronik recorder. This model has a pen speed of 1/2 second for full scale travel. The voltage span was increased, here, to a 4 volt span by means of a potential divider. For the resistances used in this divider, the recorder requires 0.8 microampere/ volt. The basic paper speed of the recorder is 2"/second, with gear changes allowing 1, 3, and 4"/second. A microammeter and a precision resistor were placed in the measuring circuit to determine the recorder current when necessary.

A 1.2 V bucking potential, tapped from a potential divider across a 1.5 V battery, was placed in series with the experimental cell. This prevented a change in polarity at the input leads of the recorder when electrode potentials varied between the active and passive values.

The oxygen overvoltage potentials were measured after becoming invariant with time. The more accurate Rubicon potentiometer was used for these potential measurements, and potentials were recorded to the nearest millivolt.

Surface Area Measurements.

The true area of the iron surfaces was measured on the low area B.E.T. apparatus developed by Joncich[16] and modified especially for bulk metals by Komodromos[17]. Fifteen 7/8" circular discs were cut from the same sheet used for the electrodes. These discs were annealed and polished in the same manner as were the electrodes. Krypton was used as the adsorbate at liquid nitrogen temperatures. For these low areas, it was necessary to correct for adsorption on the walls of the glass system. Two determinations were made for the dead space, two for coupons freshly abraded with number two emery paper, and one for the coupons passivated for two hours in neutral 0.1 M Na_2SO_4. The roughness factor for the glass was measured with the area of two concentric test tubes which were sealed at the

top, and the bottom of the outer tube was connected to the dead space. This gave a large surface area to dead space volume ratio. The results are given below.

Table 1

Sample	Condition	Roughness Factor
Dead Space	Washed in Soap	1.8, 2.0; avg., 1.9
Iron Coupons	Abraded	2.7, 2.9; avg., 2.8
Iron Coupons	Passivated	7.7

Experimental Results for Anodic Polarization Phenomena

To present the experimental results, it is best to refer to Figure 2 which is a typical time-potential trace of an iron electrode being polarized alternately anodically and cathodically. The pH of the solution was 11.6 for this experiment. The anodic current causing the potential change from A to C or G to C' was about 10 mA/A.cm.^{2} The potential change from C' to H came about when the anodic current density was suddenly reduced from 10 to 0.1 mA/A.cm.^{2}

The potential arrests in these curves are indicative of chemical reaction, e.d.l. buildup, or e.d.l. decay. The potential of the arrest is determined by the reaction proceeding at the electrode, and the period of existence of the arrest depends on the amount of reaction occuring.

No extensive studies were made of the potential arrests labeled A, B, B', G, and G' for it was felt that processes occurring at these potentials were not of primary interest to this work.

Open Circuit Potential (A)

The potential (A) is obtained on placing the electrode in solution with no external anodic or cathodic polarization. In these experiments, the measured potential is not quite the open circuit potential. At the usual recorder reading, a cathodic current drain of about 0.5 uA is necessary for operation of the recorder. The potential measured under these conditions is 5 to 10 millivolts more negative than the same potential measured on a very high resistance potentiometer.

The open circuit potential of an electrode is complex in most cases, and the iron electrode is no exception. A typical iron surface contains regions of relatively high electrochemical reactivity. These regions are anodic with respect to the more inactive regions of the surface, i.e., the cathodic areas. The current passing between the local anodes and cathodes polarizes both to approximately the same potential, and this is the open circuit (or "mixed") potential of the iron electrode under normal conditions.

The open circuit potential of the electrodes was not studied to any extent. Qualitatively, the potential varied

Figure 2. Potential - Time traces for the build up
and decay of oxygen evolution in basic
solution.

VOLTS

−0.8
−0.4
0.0
+0.4
0.8
1.2
1.6
2.0

SECONDS

1 2 3 4 5 6 7 8 9

A B C D E F G B' C' D' E' H H' G'
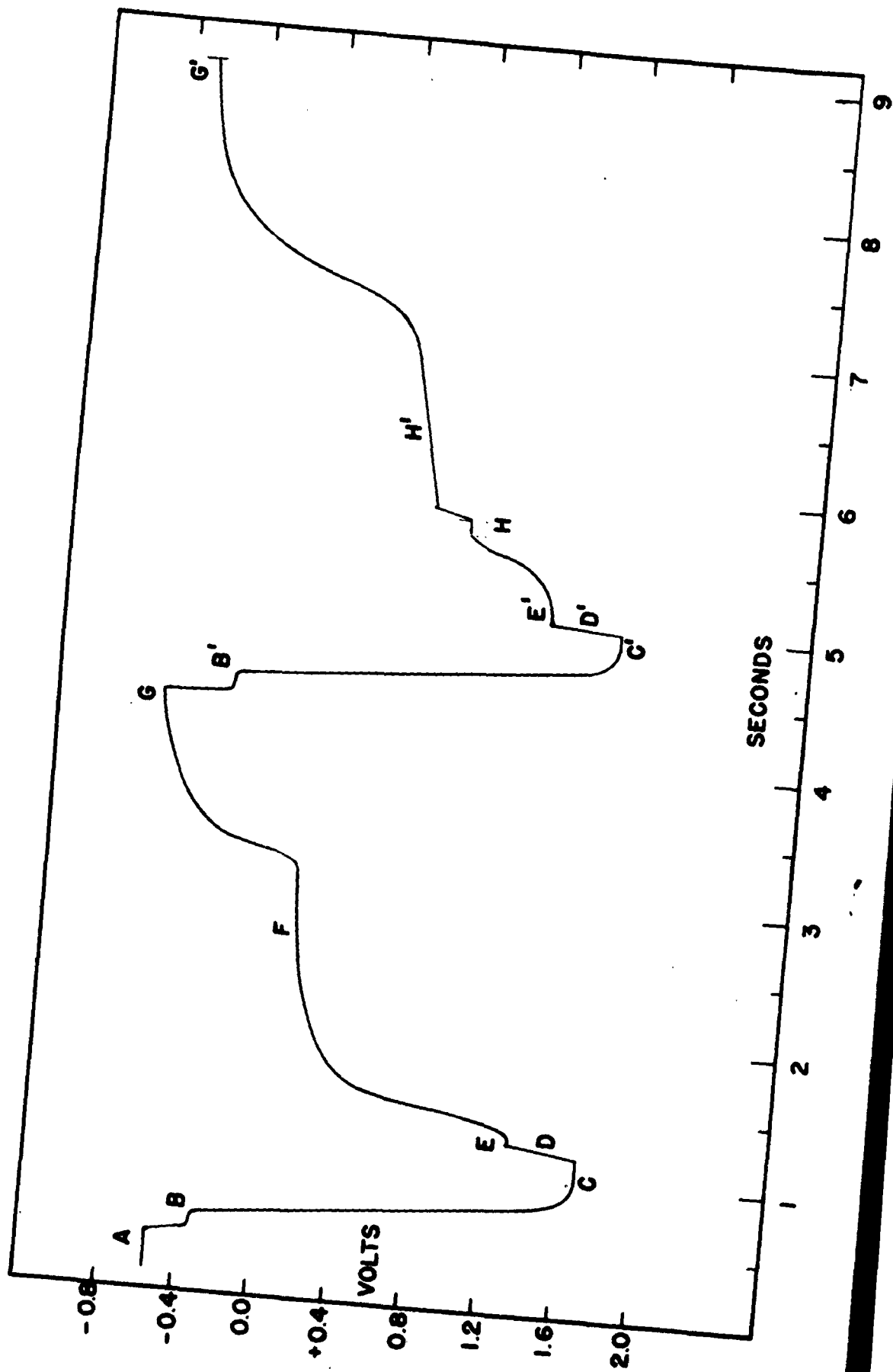
from -0.7 to -0.4 volts depending on the pH of the solution, the potential varying directly with pH.

Anodic Dissolution of Iron (B)

With the potential of the electrode at A, anodic polarization was applied. If the current was sufficiently large, the potential eventually came to the oxygen evolution potential, C. In going from A to C, a potential arrest was found at B, corresponding to the polarized anodic dissolution potential of iron-ferrous ion.

Mueller[5,6] found that passivation is preceeded by passage of a certain number of coulombs, which depends on the experimental conditions. For instance, it varies directly with stirring rate and inversely with pH of the solution. These observations led him to conclude that dissolution of some quantity of iron is an integral step in the passivation process. He postulated that, for sufficienty high current densities, the transfer of ferrous ions to the bulk of solution is under diffusion control. This allows the concentration of ferrous ions in the vicinity of the electrode to increase until the solution is saturated. At this point, precipitation of ferrous salts on the surface of the electrode masks most of the surface, causing a large increase in current density. To allow for this increase in current density, the potential increases in a positive direction. Eventually the potential will rise to the oxygen evolution potential. Only then will oxygen be evolved. Bartlett and Stephenson[16] have used a Schleren microscope to observe directly the dissolution of metals. They are able to follow the changes in concentration of the dissolution products in the vicinity of the electrode.

It was easily possible to verify the postulates of Mueller qualitatively. In a solution of pH 2.5, the number of coulombs necessary for passivation was found to be about 100 times the number required for a solution of pH 12. Similarly, increased stirring rates required the expected increase in the number of coulombs passed prior to passivation.

Oxygen Evolution (C)

When the potential of the anodically polarized electrode passed from B to C, oxygen evolution commenced. Potential C is the steady state oxygen evolution potential. This potential was measured as a function of the current density and solution pH. The experimental procedure for each pH studied was to : A) passivate the coupons at 20 mA/A,cm.^{2} for two hours, B) switch to the 90 volt battery for the measurements, C) vary the anode current by interchange of series resistors, and D) measure the potential at each current setting.

At the same pH it is expedient to measure a whole series of points on only one coupon. The difficulty with this procedure is that the freshly abraded coupons slowly roughen with passivation time. This produces a continous variation in the current density due to the changing surface area. The procedure adopted here was to purposely roughen the coupons by passivation for two hours at 20 mA/A.cm.^{2}. The coupons which showed a roughness factor of 7.7 (Table 1) were treated in the same manner. It was felt that in this length of time, the coupons would reach a maximum roughness. There is no independent verification of this assumption; however, Figure 3 demonstrates its validity. Experimental points for each of the curves were not taken in sequence. The smoothness of the curves is indicative of an unchanging electrode area.

After switching to the 90 volt battery, the potential of the electrode was measured at 15 minute intervals. When the potential changed by less than 0.2 millivolt over one of these intervals, it was recorded. Forty-five to sexty minutes were usually required to obtain the steady state. Some potentials were followed for as long as five hours, and no change was found after the first hour.

Oxygen Overvoltage at pH 9.5, 11.0, and 12.2

Figure 3 shows the variation of the measured electrode potential, E_m, with logarithm of true current density for solutions of pH 9.5, 11.0, and 12.2. These curves approach Tafel's linear relationship only at the high and low current densities. The three curves indicate that there is a combination of resistance, concentration, and activation polarization.

Resistance Overvoltage.

Since resistance polarization is of little theoretical importance to the nature of the electrode reaction, it is only necessary to eliminate it. It is neither desirable nor possible to place the capillary tip of the reference electrode against the surface of the electrode, and therefore appreciable ohmic overvoltage occurs at the higher current densities.

The particular design of this cell made it impossible to correct for this by extrapolation of potential-distance curves to zero distance. However, using the recording potentiometer, it is possible to calculate the ohmic overvoltage by another method. If the anodic polarization is allowed to decay, an almost instantaneous drop is observed as the first step. This drop is labeled D in Figure 2. True ohmic overvoltage decays instantaneously. On the 1/2 second recorder, a small time (about 1/10 second) is required for this decay. However, the decay time does not vary with the cathodic decay current

Figure 3. Measured oxygen overvoltage curves
for solutions of pH 9.5, 11.0 and 12.2

VOLTS

pH = 9.5

pH = 11.0

pH = 12.2

LOG (A/T.CM.^{2})

1.6 1.4 1.2 1.0 0.8 0.6
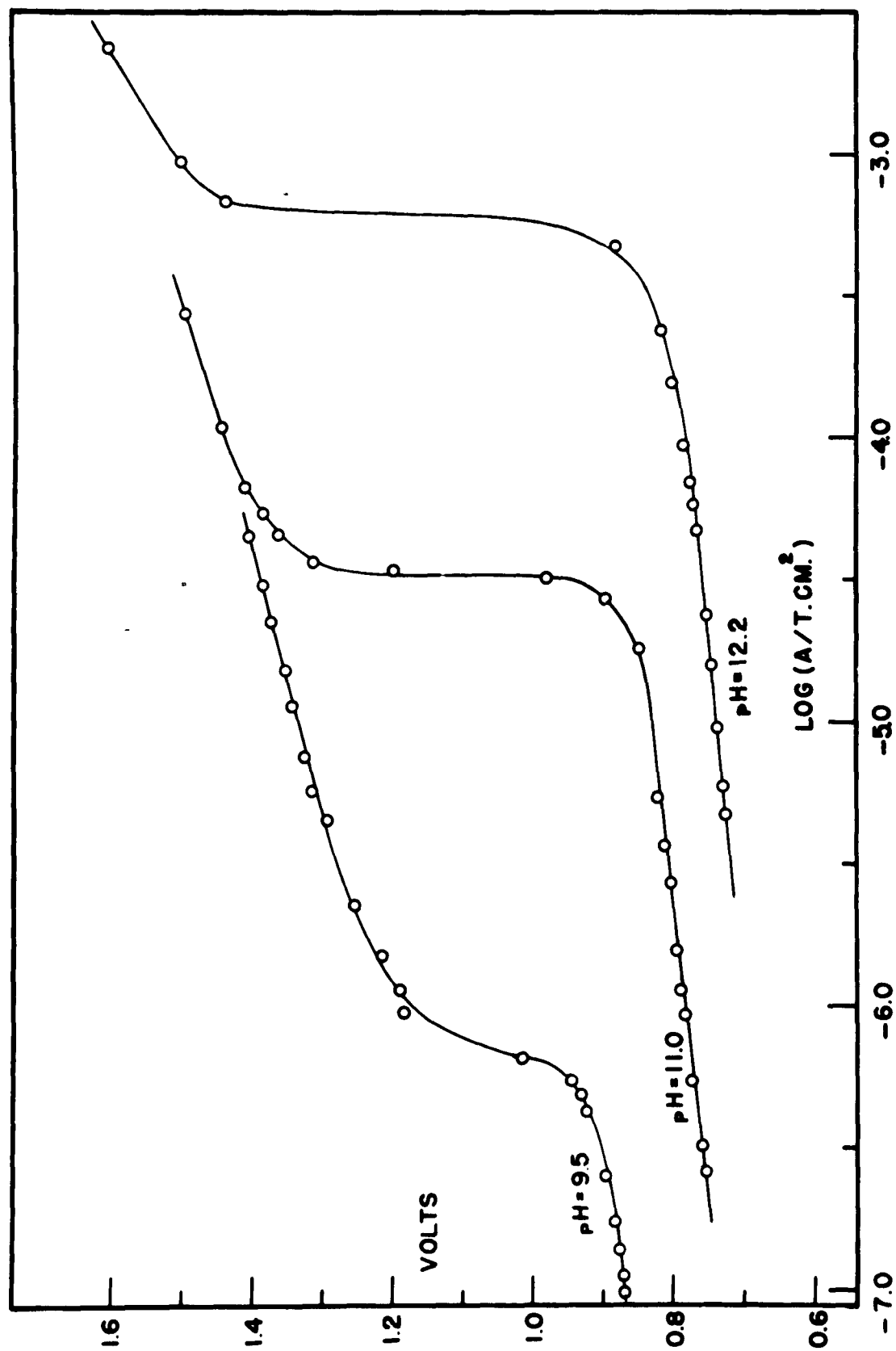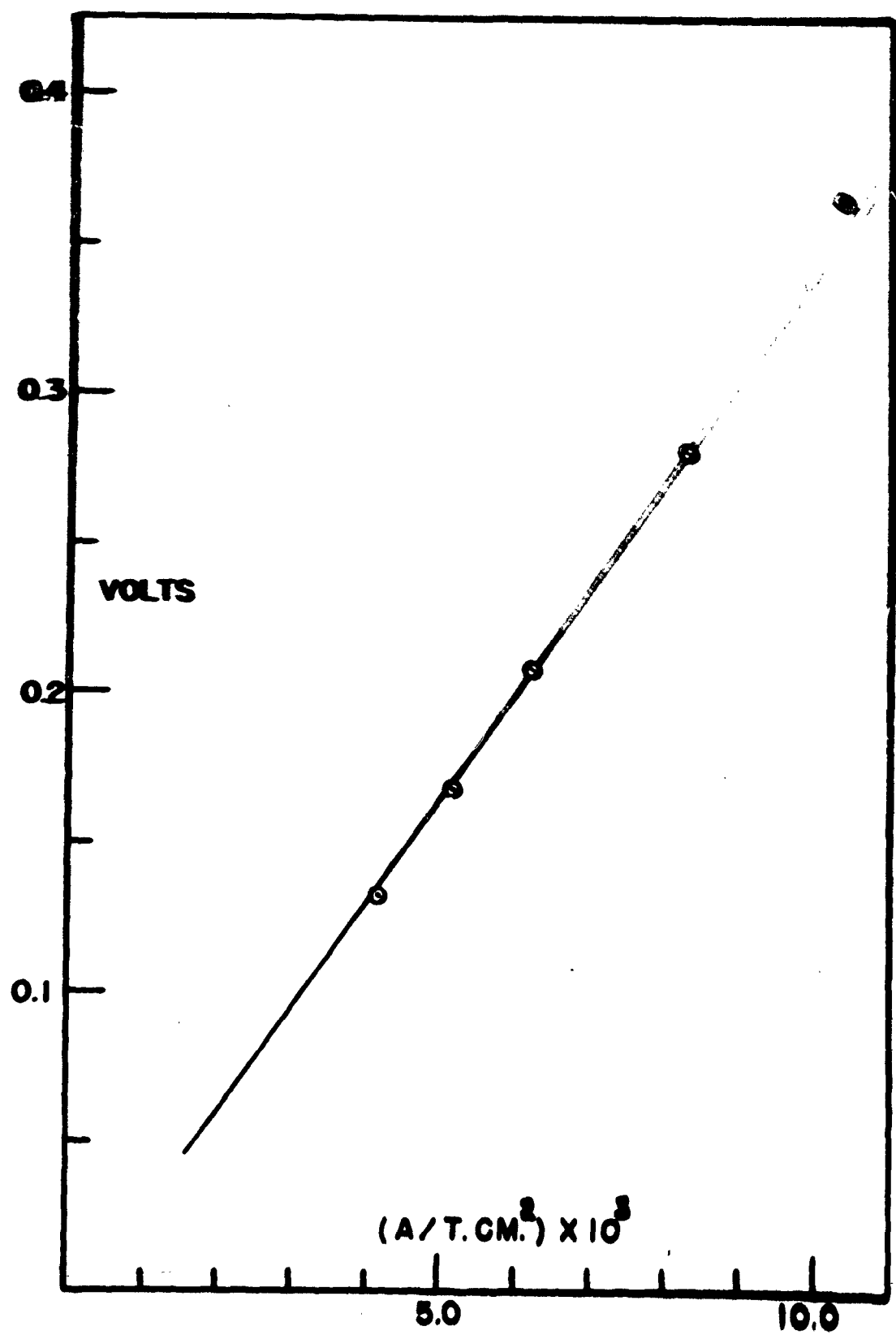
-7.0 -6.0 -5.0 -4.0 -3.0

Figure 4. Ohmic overvoltage as a function of the
anodic current density-pH of 12.2.

as would be expected if the potential drop D required the passage of charge. The decay D is instantaneous as far as the recorder is concerned.

A plot of this IR drop versus the anodic current density prior to decay should give a straight line. Figure 4 shows such a plot for the pH 12.2 solution. The slope of this line is the ohmic resistance per cm.^{2} of true area. Multiplication of this resistance by the true anodic current density gives the ohmic overvoltage at any current density. Currents on the order of 10 to 50 mA/T.cm.^{2} are used to obtain measurable potential drops (D) on the recorder

For solutions of pH 9.5 and 11.0 similar plots were constructed from the experimental data. The determination of these slopes was made just before the overvoltage measurements. The following table lists the slopes of the linear plots for the three solutions.

Table 2

pH	Slope (volts/amp./T.cm.^{2})
9.5	15.0
11.0	36.6
12.2	33.4

Calculation and subtraction of the ohmic overvoltage for each of the experimental points of Figure 3 results in the curves of Figure 5. Figure 5 shows that the corrections help linearize the upper potential steps of the curves of Figure 3.

Concentration Polarization:

The evolution of oxygen from unbuffered aqueous solutions can easily lead to concentration polarization. When the diffusion of hydroxyl ions to the electrode is slower than is their discharge rate, the pH at the surface decreases. The equation* for the change in OH^- concentration

$$\Delta OH^- = 10^3 \frac{\delta}{D_{OH^-} F} I \qquad (I)$$

holds while the solution at the surface of the electrode is still alkaline. Here, is the thickness of the diffusion layer, D_{OH^-} is the diffusion coefficient for hydroxyl ion, F is the Faraday, and I is the apparent current density. δ is about

* This treatment is given by King.[19]

5×10^{-3} cm. for solutions stirred by bubbling gas, and D_{OH^-} is approximately 4×10^{-5} equivalents/A.cm.^{2} sec. The apparent area is used for calculation of current densities because the depth of abrasion scratches on the electrode surface is usually small compared to δ.

For current densities sufficiently large to acidify the diffusion layer, calculations must be made on the basis of the increase in hydrogen ion concentration at the surface. Under these conditions, the equation for the concentration of H+ at the surface is

$$(H^+)_s = \frac{\delta I/F - 10^{-3} D_{OH^-} (OH^-)_B}{10^{-3} D_{H^+}} \qquad (2)$$

where $(OH^-)_B$ is the bulk concentration of hydroxyl ion, D_{H^+} is the diffusion coefficient of hydrogen ions, and the other symbols have the same significance as in Equation (1).

The difference of potential for a chemical species (A) in two different phases (1 and 2) is given by

$$\Delta E = -\frac{RT}{F} \ln \frac{(A)1}{(A)2} \qquad (3)$$

The concentration overvoltage for electrode systems with an alkaline diffusion layer is given by

$$\Delta E_c = -\frac{RT}{F} \ln \frac{(OH^-)_B - 10^{-3} \delta/D_{OH^-}F}{(OH^-)_B} \qquad (4)$$

For systems with an acidic diffusion layer, the concentration overvoltage is

$$\Delta E_c = -\frac{RT}{F} \ln \frac{\delta I/F - 10^{-3} D_{OH^-}(OH^-)_B}{10^{-3} D_{H^+}(H^+)_B} \qquad (5)$$

A plot of ΔE_c as a function of log I is identical to a potentiometric titration curve with the volume reagent added replaced by log I. The potential steps in Figure 5 are of the approximate height to be explained by concentration overvoltage. Subtraction of the calculated concentration overvoltage should result in the linear Tafel plot for activation polarization.

For a completely valid calculation of the extent of concentration overvoltage for the three pH solutions, the following must be known: (1) The bulk pH: this was measured on a Beckman pH meter, (2) Independently determined values for δ and D. Normally, independent determinations of the parameters and D are involved and were not considered necessary for this

Figure 5. Oxygen overvoltage as a function of the
logarithm of true current density, after
subtraction of ohmic overvoltage.
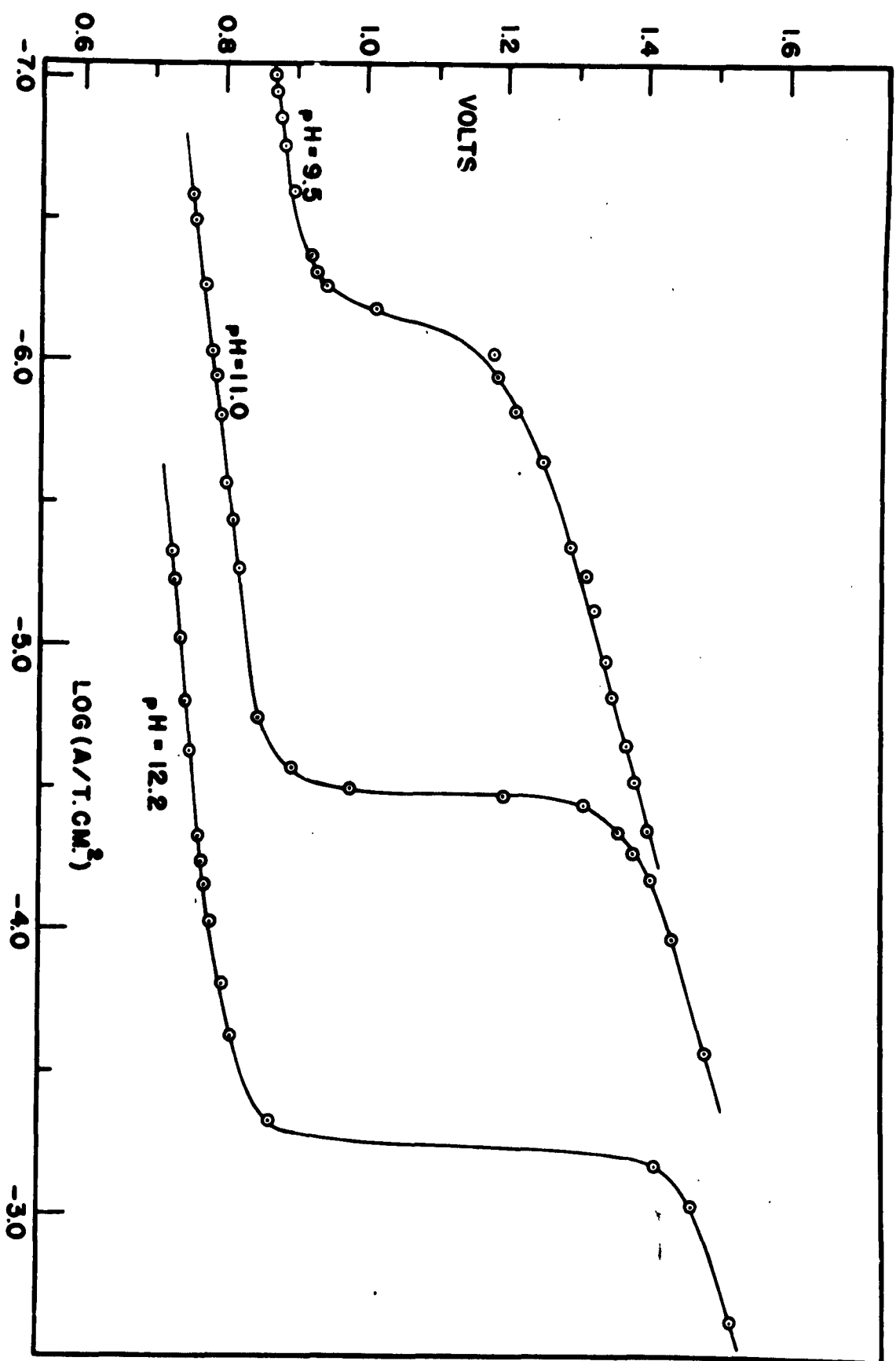
work. The apparent current density at which the potentirl step occurs is the limiting current density (l.c.d.). At the l.c.d., the $(OH^-)_s$ falls almost to zero. Thus ΔOH^- is almost equal to the bulk concentration of hydroxyl ion. Substitution of this value and the l.c.d. into Equation 2 yields the ratio of δ/D_{OH^-} . More uncertainty exists in the value of than in the value of D_{OH^-} due to the marked variation of δ with stirring rate. The diffusion coefficient for H^+ or OH^- can be assigned the value of 4×10^{-5} with reasonable certainty, and, hence, δ can be calculated. Table 3 lists l.c.d., δ , and 10^3 δ/D_{OH^-} F for each solution pH.

Table 3

pH	l.c.d.(A/A.cm.^{2})	δ	10^3 δ/D_{OH^-} F
9.5	5.069×10^{-6}	4.44×10^{-3}	1.15
11.0	2.49×10^{-4}	2.86×10^{-3}	0.741
12.2	4.33×10^{-3}	2.81×10^{-3}	0.728

Using King's values of 5×10^{-3} and 4×10^{-5} for δ and D_{OH^-}, equation (2) gives

$$\Delta OH^- = 1.25 \ I \qquad\qquad (6)$$

The agreement of the values of Table 3 with Equation (6) is good considering the large variations that King found in his determinations of δ . The constancy of δ or the linear variation of log(l.c.d.) with pH gives strong indication that the potential steps of Figure 5 arise from concentration polarization. Also, it was repeatedly observed that increased bubbling rates shifted the l.c.d. to larger values. Undoubtedly, the variations that do exist in δ are due to the inability to reproduce the conditions of stirring.

Assuming $D_{OH^-} = D_{H^+} = 4 \times 10^{-5}$ and using the values of Table 3, the concentration polarization was calculated from equations (7) and (5) for the three solutions. For the purposes of calculation, the true current density for each point in Figure 5 was first converted to the apparent current density. Figure 6 shows the calculated concentration overvoltage as a function of $log(A/T.cm.^2)$ for the pH 9.5 solution. The concentration for all three solutions were subtracted from the experimental curves of Figure V. The elimination of concentration overvoltages results in Figure 7.

The potential steps were not quite eliminated; however, both the upper and lower sections are linear and of approximately the same slope. An explanation for the residual step is offered later.

Figure 6. Calculated concentration overvoltage as
           a function of the logarithm of apparent
           current density for a solution of pH 9.5.
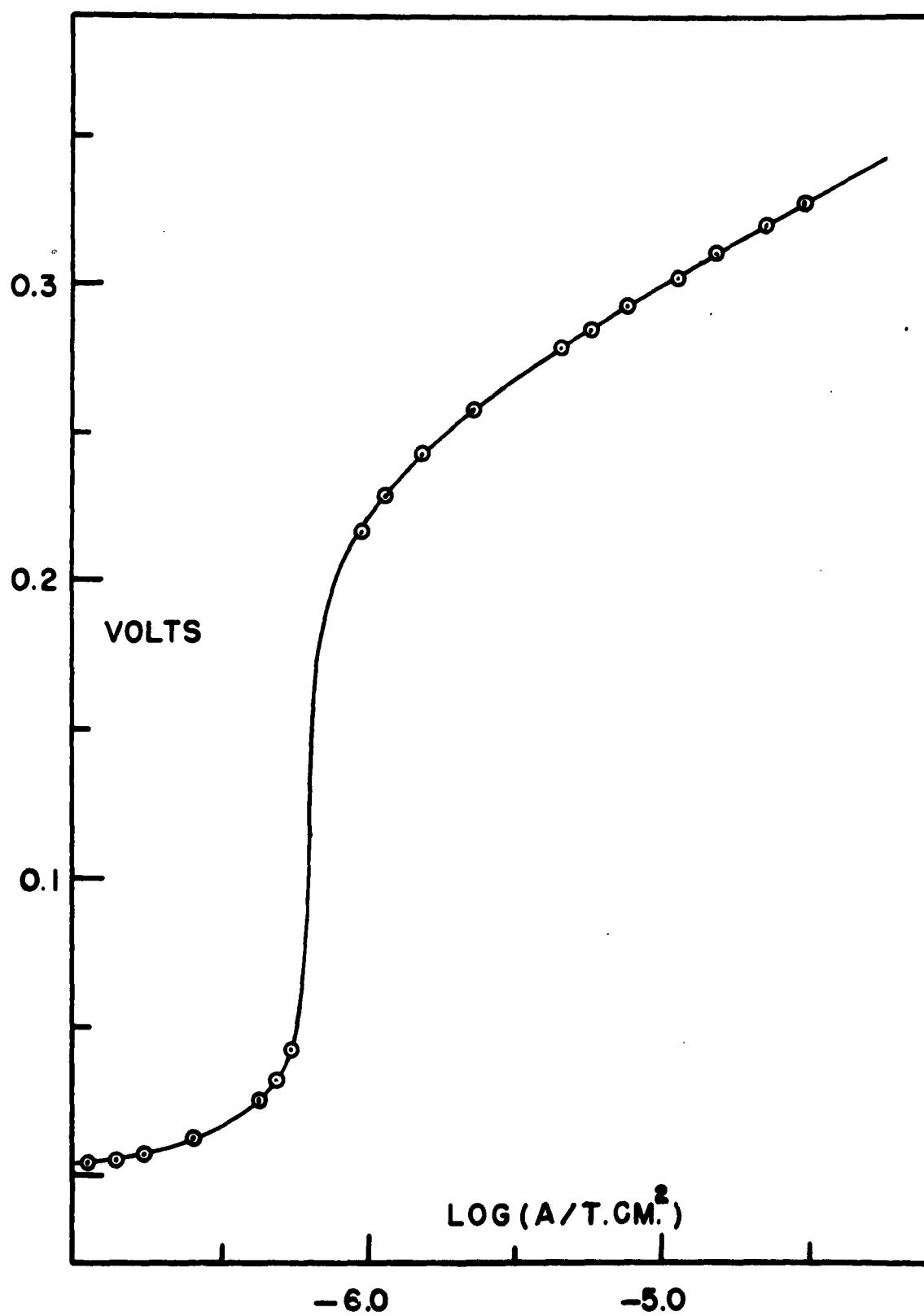
Activation Polarization

The residual curves of Figure 7 are Tafel plots for activation polarization. The activation polarized potentials, E_a, are converted to overvoltages, η, by subtraction of the reversible oxygen potential appropriate to each pH. The reversible oxygen potential as a function of hydroxyl ion concentration is

$$E_{R_{O_2}} = 0.143 - 0.055 \; Log \; (OH^-) \qquad (7)$$

at $5°$ C. relative to the saturated calomel electrode. The constants a, a', and b of the upper and lower sections of the Tafel curves

$$E_a = a + b \; LogI \qquad (8)$$

and

$$\eta = a' + b \; LogI \qquad (9)$$

are listed in Table 4, with the reversible oxygen potentials. The signifigance of these data is more appropriately discussed later.

Oxygen Overvoltages at pH 2.5, 4.0, and 14.5.*

Although the preceeding data have afforded a good demonstration of concentration resistance overvoltage effects, the resulting Tafel curves are still unstaisfactory. This is due to the large corrections needed, except at low current densities. To obtain more accurate activation overvoltage curves, it is best to (a) Utilize the self-buffering action of either high or low pH solutions to minimize concentration polarization and (b) Work at smaller current densities to minimize resistance polarization. The results of experiments under these more rigorous conditions are shown in Figure 8. These Tafel curves have been corrected for concentration and resistance overvoltage where necessary. The largest correction applied to the pH 2.5 or 14.5 curves was 10 millivolts. The pH 4.0 curve required somewhat larger corrections. For these small concentration overvoltage corrections, it was considered unnecessary to redetermine δ. The average of Table 3 was used with the bubbling rates reproduced as closely as possible. The constants of Equations (8) and (9) which fit these linear

---

* The pH of 14.5 was calculated for a solution 1.0 M in NaOH and 0.1 M in Na_2SO_4, having an activity coefficient of 0.650. For this solution, there was no pre-roughening treatment, and it was observed that the coupons did not roughen. The roughness factor of 2.8 was used in the calculations of the true current density.

Figure 7. Activation overvoltage versus logarithm
of true current density for solutions of
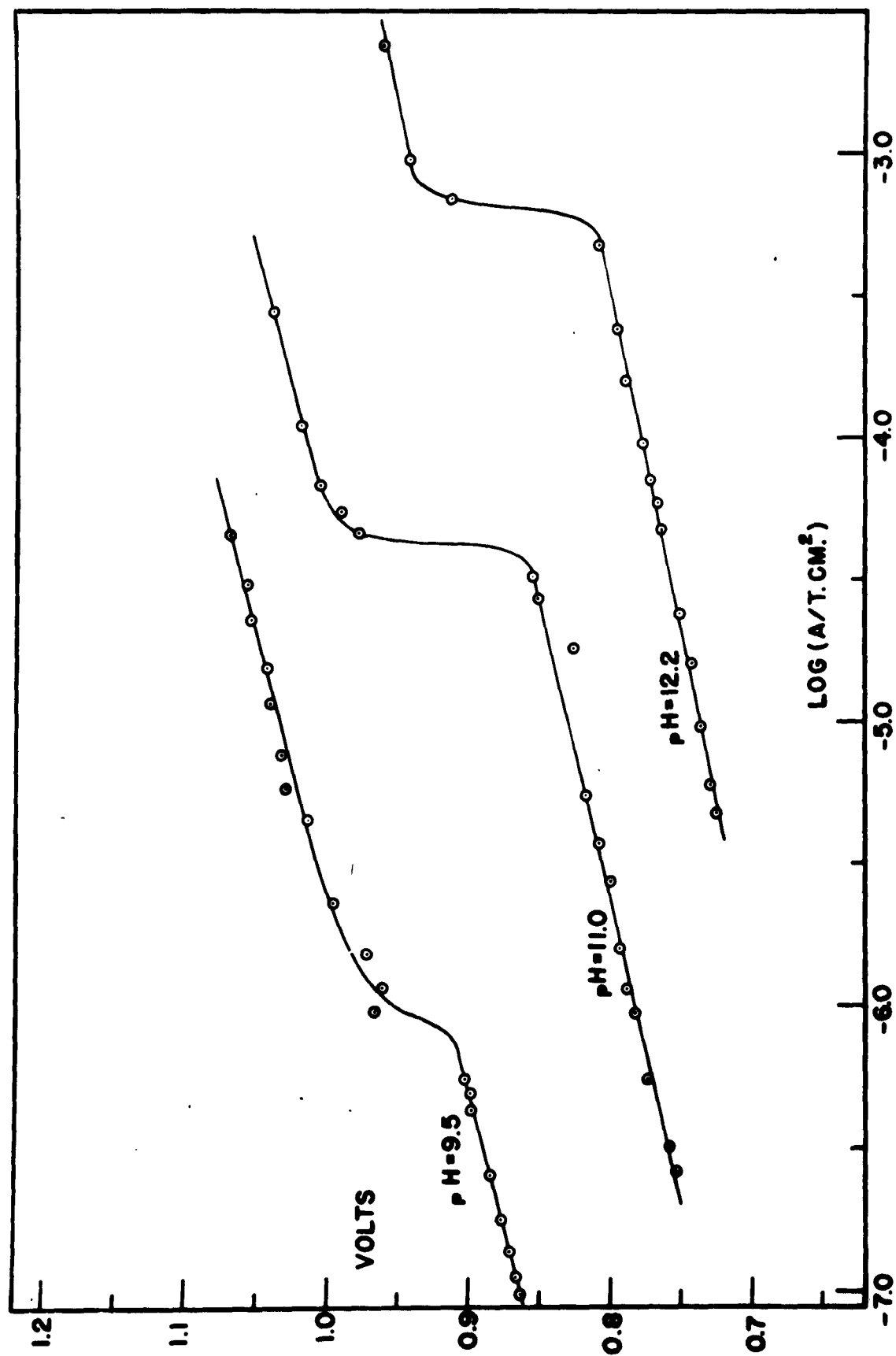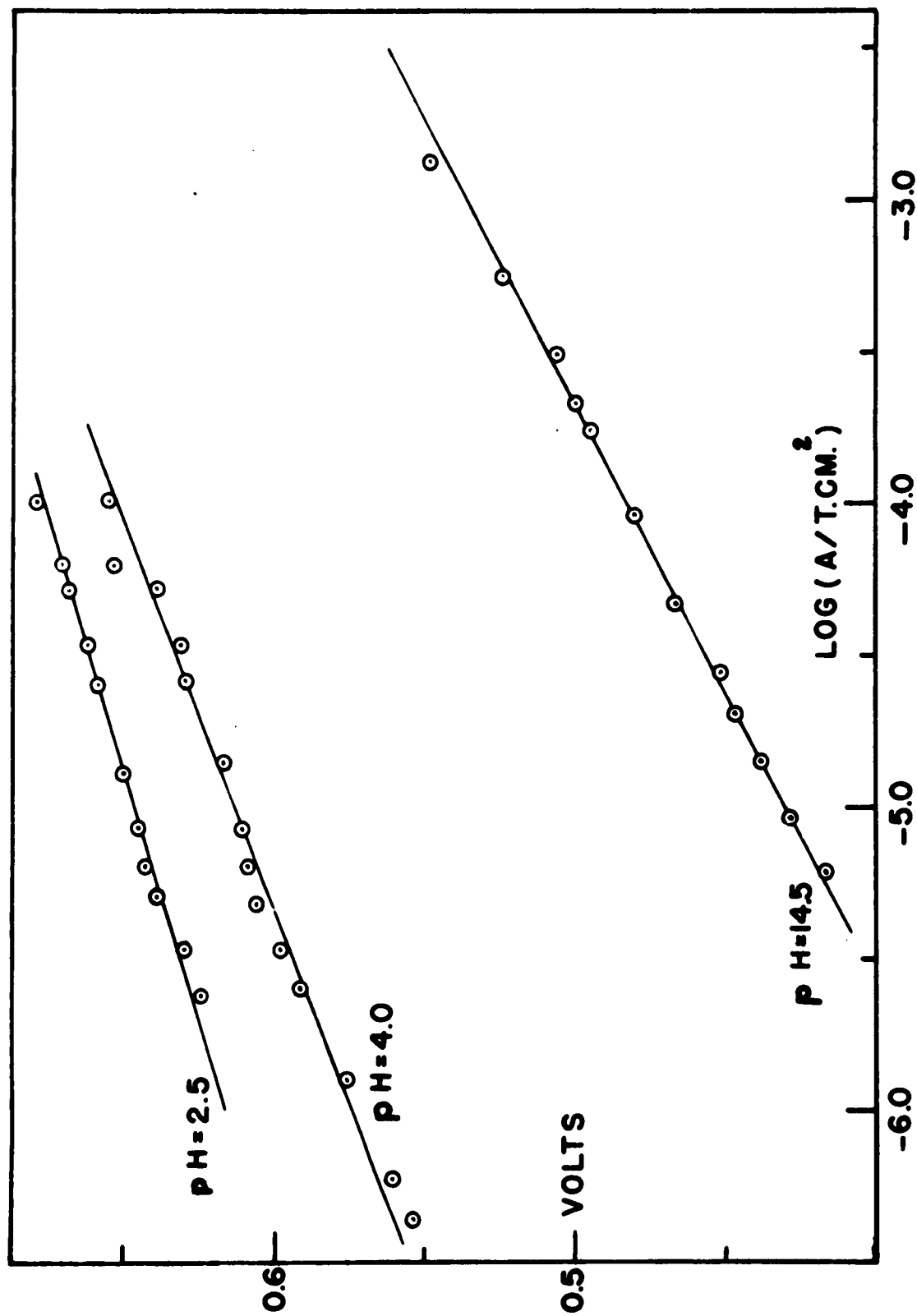pH 9.5, 11.0, and 12.2.

VOLTS

pH=9.5

pH=11.0

pH=12.2

LOG (A/T.CM^2.)

Figure 8. Activation overvoltage versus logarithm
of true current density for aolutions of
pH 2.5, 4.0, and 14.5.

curves are given in Table 4.

Discussion of Oxygen Evolution

Table 4 is a compilation of data gathered from the Tafel curves at the various pH's. Excluding the upper sections of the Tafel curves, two general trends are noticed. First, the slopes are different in acidic and basic solution. This is indicative of a change in reaction mechanism. Secondly, the constant a' generally increases with decreasing pH. This effect is offered as the explanation of the anomalous potential steps of Figure 7.

The potential steps of Figure 7 indicate a change in the mechanism or type of anodic reaction. However, the data resulting in Figure 7 are quite complex and require large resistance and concentration overvoltage corrections to obtain the Tafel curves. Table 4 shows that, at constant current density, a' varies inversely with pH. The three columns of a' values are calculated assuming current densities of 1, 10^{-3}, and 10^{-6} A/T.cm.^{2}. The a' values are the total overvoltages at those current densities. Figure 9 is the plot of these a' variations with pH for each of the units of current density. The changes in pH in the regions of the potential steps are about 4, 6, and 8 units (pH 9.5, 11.0, and 12.2). Figure 9 shows qualitatively that these surface pH changes alter a' sufficiently to explain the residual steps in Figure 7.

Bokris[20], in developing the theory of activation overvoltage, points out the necessity for certain parameters not discussed here, to remain constant. These parameters are included in a'. For a linear variation of overvoltage with the logarithm of current density, either a' must be independent of the current density, or a' must have a logarithmic dependency on current density. The second condition cannot easily be given a theoretical treatment. Often a' is found to be independent of pH over wide ranges, as in the evolution of oxygen off a platinum surface.[21]

The upper sections of the curves of Figure 7 can be considered in another manner. The surface pH conditions that existed for the upper sections of these curves are similar to the conditions in solutions of pH 2.5 and 4.0. Table 4 shows that the a' constants for these two cases are approximately the same. Therefore, indications are that the potential steps of Figure 7 do not signify a change in the type or mechanism of the anodic reaction.

A closer inspection reveals that the previous conclusion is probably not tenable. The removal of the potential step does not eliminate the possibility that the mechanism of the upperstep differs from the mechanism of the lower step. The slopes of the Tafel curves in acid solution differing from those in alkaline solution indicate a change in the mechanism

TABLE IV

pH	$E_{R_{O2}}$	b	Lower a(A)	a'(A)	a'(mA)	a'(uA)
14.5	0.153	0.054	0.852	0.699	0.537	0.375
12.2	0.277	0.046	0.962	0.685	0.547	0.409
11.0	0.349	0.046	1.060	0.711	0.573	0.435
9.5	0.432	0.052	1.228	0.796	0.640	0.484
4.0	0.736	0.040	1.550	0.824	0.704	0.584
2.5	0.818	0.030	1.614	0.796	0.706	0.616

pH	$E_{R_{O2}}$	b	Upper a(A)	a'(A)	a'(mA)	a'(uA)
12.2	0.277	0.045	1.080	0.803	0.668	0.533
11.0	0.349	0.049	1.215	0.866	0.719	0.572
9.5	0.432	0.045	1.264	0.832	0.697	0.562

Figure 9.   Variation of the a' constants of the Tafel
equation with pH.
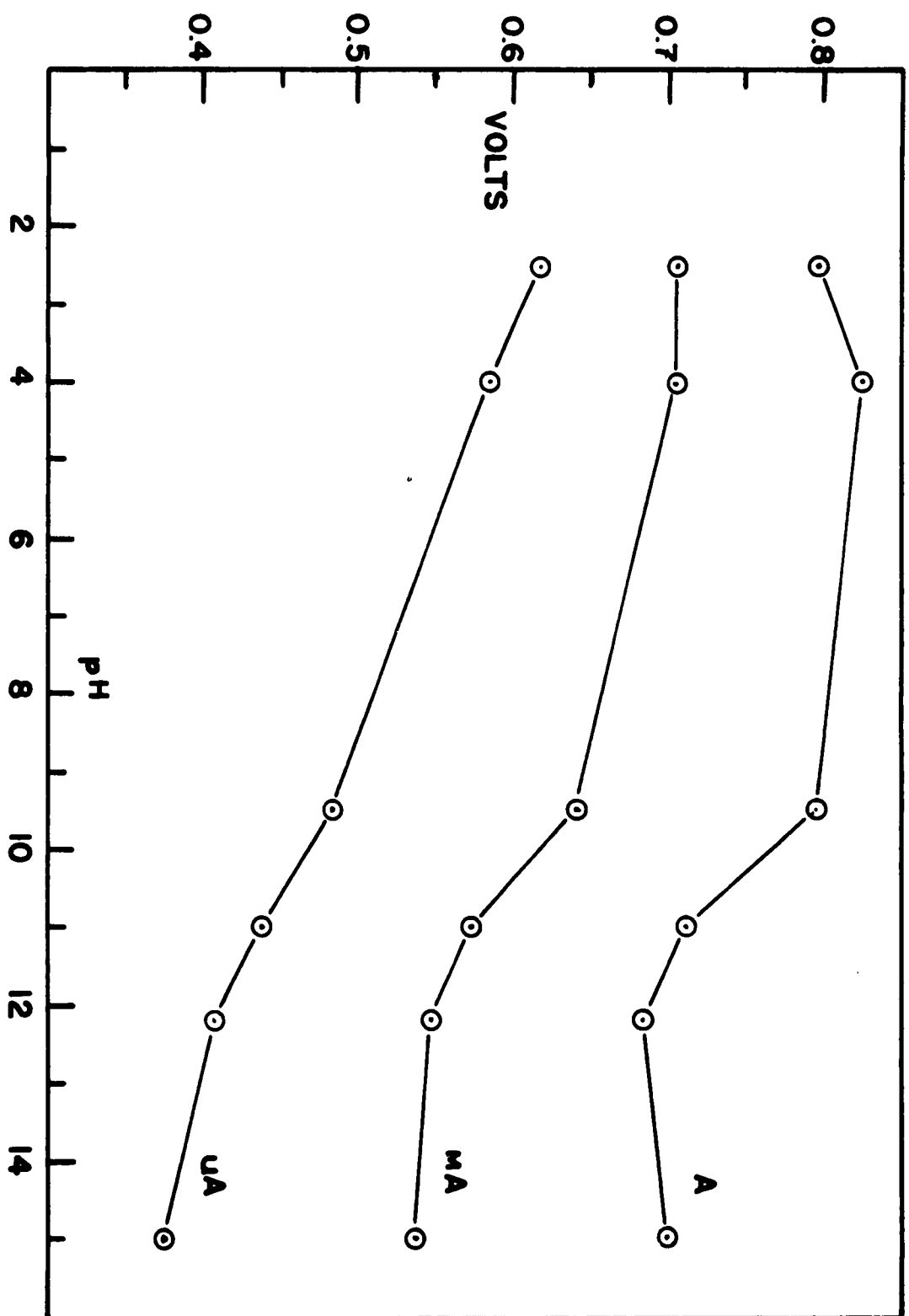
of the reaction. The slopes of the upper sections in Figure 7 agree more closely with those in alkaline solution. When the solution at the electrode is acid, the slopes should a-gree with those in acid solution. There are several reasons for this disagreement.

First, there is a pH variation over the range of current densities of the upper sections. For instance, at pH 9.5, there is a variation of 2 units. Figure 9 shows that, in acid solution, a' increases with decreased pH over the current density range studied. It is impossible to say whether a pH change of 2 units is sufficient to reduce the slope to a value compatible with the bulk acid solutions. However, corrections of slopes would be in the direction of the values for acid solution.

Second, when the experimental data were taken, the primary interest was on the concentration overvoltage effects. For a more accurate interpretation of the upper slopes, the experiments will have to be extended.

The more valuable and valid conclusions pertaining to activation overvoltage were obtained from the solutions of pH 2.5, 4.0, and 14.5. The slopes of the Tafel curves in these three solutions are 0.030, 0.040, and 0.054 respectively. The measurements at pH 4.0 are the least useful due to the extent of some of the corrections. Theoretical treatments[22] show that the slope of the Tafel curve is closely related to the specific mechanism of the electrode reaction. This fur-nishes an excellent means of investigation of electrode kine-tics. Each rate determining step in the electrode reaction provides a characteristic value for the Tafel slope, which is an integral multiple of $2.303 RT/F$. Table 5 lists the more probable mechanisms for oxygen evolution along with the theo-retical slopes, b, and the stoichiometric number, γ. The b values are calculated for $25°$ C. assuming a symetrical po-tential energy barrier, and ν is the number of times that the rate determining step occurs when the over all reaction oc-curs once. An experimental determination of both b and ν is sufficient to characterize the exact mechanism. the determi-nation of ν requires measurements at current densities on the order of the exchange current. Potential measurements at these currents are very tedious.

The experimental value of 0.030 at pH 2.5 agrees well with step 2 in mechanisms 1, 4, or 6. It should be noted that the parameters associated with the mechanisms are the same re-gardless of whether hydroxyl ions are discharged or water mole-cules are discharged in the first steps. Mechanisms 4 or 6, however, are improbable since in acid solution, the hydroxyl ion concentration suggests that step 3 of each mechanism is unlikely. Therefore, the mechanism of oxygen evolution at pH 2.5 is believed to be:

    1. Discharge of H_2O to give hydroxyl radicals ad-sorbed on the surface.

TABLE 5

Mechanism*	b	ν
1. $4OH^- \to 4M\text{-}OH + 4e_o^-$	0.110	4
$\quad 4M\text{-}OH \to 2M\text{-}O + 2M + 2H_2O$	0.028	2
$\quad 2M\text{-}O \to 2M + O_2$	0.014	1
2. $2OH^- \to 2M\text{-}OH + 2e_o^-$	0.110	2
$\quad 2M\text{-}OH + 2OH^- \to 2M\text{-}O + 2H_2O + 2e_o^-$	0.036	2
	or 0.110	2
$\quad 2M\text{-}O \to 2M + O_2$	0.014	1
3. $4OH^- \to 4M\text{-}OH + 4e_o^-$	0.110	4
$\quad 2M\text{-}OH \to 2M + M\text{-}H_2O_2$	0.014	1
$\quad M\text{-}OH + M\text{-}H_2O_2 \to H_2O + M\text{-}HO_2$	0.014	1
$\quad M\text{-}HO_2 + M\text{-}OH \to 2M + O_2 + H_2O$	0.014	1
4. $2OH^- \to 2M\text{-}OH + 2e_o^-$	0.110	2
$\quad 2M\text{-}OH \to M\text{-}O + M + H_2O$	0.028	1
$\quad 2M\text{-}O + 2OH^- \to 2M\text{-}O\text{-}OH + 2e_o^-$	0.110	2
$\quad 2M\text{-}O\text{-}OH \to M\text{-}O + M + H_2O + O_2$	0.014	1
5. $4OH^- \to 4M\text{-}OH + 4e_o^-$	0.110	4
$\quad 2M\text{-}OH \to M\text{-}O + H_2O$	0.014	1
$\quad M\text{-}O + M\text{-}OH \to M\text{-}O\text{-}OH$	0.014	1
$\quad M\text{-}O\text{-}OH + M\text{-}OH \to M + H_2O + O_2$	0.014	1
6. $2M\text{-}OH^- \to 2M\text{-}OH + 2e_o^-$	0.110	2
$\quad 2M\text{-}OH \to M + M\text{-}O + H_2O$	0.028	1
$\quad M\text{-}O + 2M\text{-}OH^- \to 3M + 2e_o^- + O_2 + H_2O$	0.055	1
7. $2M\text{-}OH^- \to M\text{-}O + H_2O + 2e_o^-$	0.055	1
$\quad M\text{-}O + 2M\text{-}OH^- \to 3M + 2e_o^- + O_2 + H_2O$	0.055	1

* The first five mechanisms are taken from Bokris[20].

2. Conversion of the hydroxyl radicals to adsorbed oxygen atoms. This is the slow step.
3. Combination and simultaneous discharge of oxygen atoms.

The slope of the Tafel curve at pH 4.0 is 0.040. This best agrees with the theoretical slope of 0.036 for the second step of mechanism 2. The second step in the oxygen evolution reaction is the reaction between adsorbed hydroxyl radicals and hydroxyl ions in solution. The pH of 4.0 may allow the discharge of hydroxyl ion to replace the discharge of H_2O. At pH 4.0, the mechanism is:

1. Discharge of water or hydroxyl ion to give hydroxyl radicals adsorbed on the surface.
2. Reaction between the adsorbed radicals and hydroxyl ions in solution to give adsorbed oxygen atoms.
3. Combination of adsorbed oxygen atoms with simultaneous discharge.

The experimental slope measured at pH 14.5 is 0.054 which agrees closely with the value 0.055. None of the first five mechanisms have steps corresponding to that slope. Using the notation of Bokris[22] and assuming a symmetrical energy barrier, the theoretical slope of the Tafel curve for a reaction step involving electron transfer is

$$b = 0.110 \frac{2\nu}{\eta}$$

where ν is the stoichiometric number and η is the number of electrons transferred in the reaction step. η must be twice the value of ν to obtain a slope of 0.055. This condition is satisfied only by mechanisms 6 or 7. Mechanism 7 differs from 6 only in that there is a direct oxidation of adsorbed hydroxyl ions to an adsorbed oxygen atom without going through the hydroxyl radical intermediate. Lacking further evidence, mechanism 6 is preferable because the hydroxyl radical intermediate has already been postulated in mechanisms 1 and 2. Therefore, the mechanism in strongly alkaline solution is:

1. Adsorption of hydroxyl ions on the surface.
2. Oxidation of adsorbed hydroxyl ions to adsorbed hydroxyl radicals.
3. Dehydration of two hydroxyl radicals to form an adsorbed oxygen atom.
4. Reaction between an adsorbed oxygen atom and an adjacent adsorbed hydroxyl ion to form hydrogen ion and a desorbed oxygen molecule.

Later work showed that in basic solutions there is extensive adsorption of hydroxyl ions on passive iron anodes. This fact fits well with mechanism 6 which dictates that the

Figure 10. Composite Potential-Time Decay Trace.

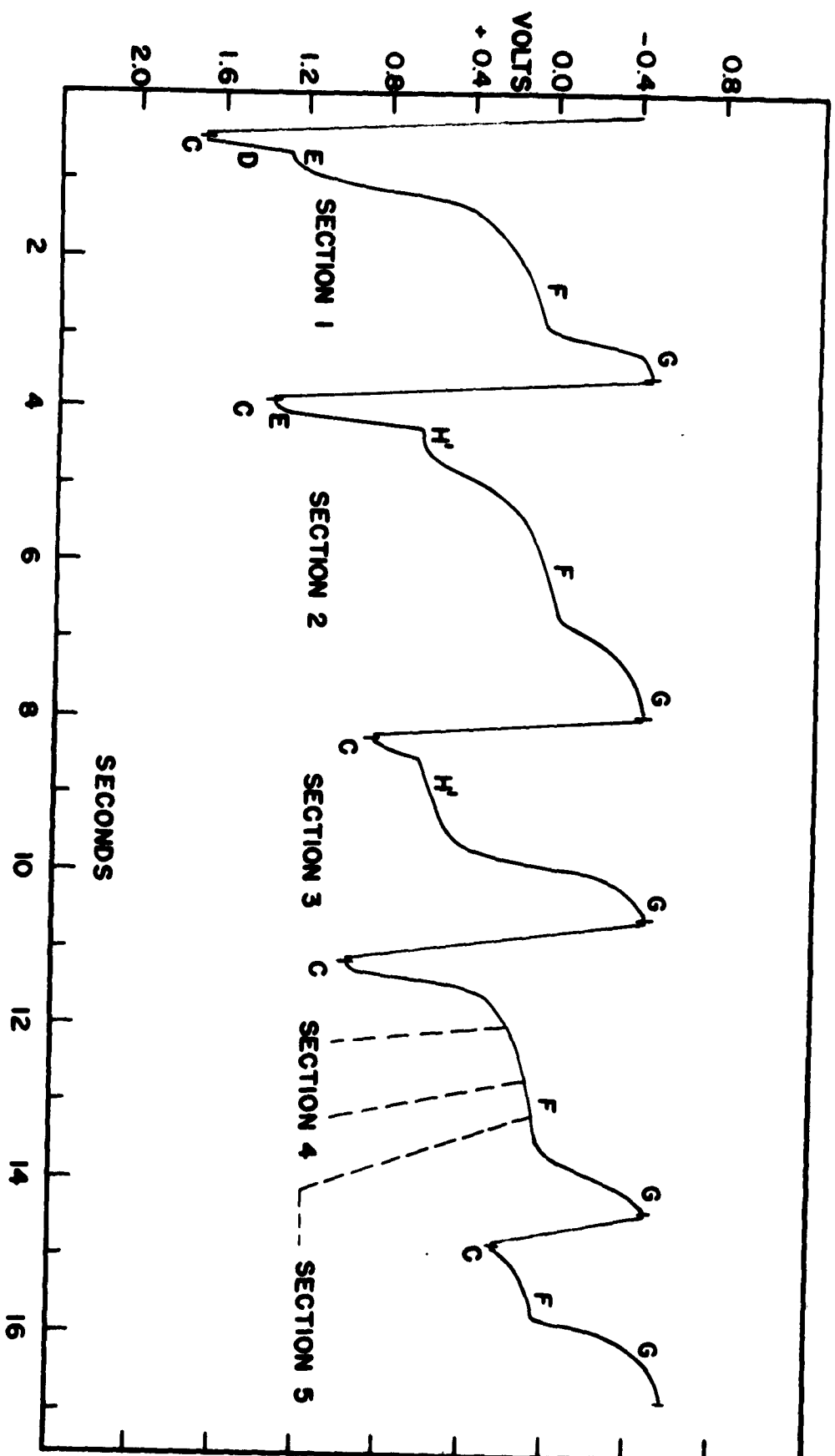Alkaline solution of pH - 11.6.

    Section 1. Decay with large concentra-
               tion overvoltage effects.

    Section 2. Decay with small concentra-
               tion overvoltage effects.

    Section 3. Decay with no concentration
               overvoltage effects.

Acid solutions of pH = 2.5

Sections 4 and 5.

concentration of adsorbed oxygen atoms is small compared to
adsorbed hydroxyl ions; otherwise, mechanism 1 would be oper-
ative with the direct combination of oxygen atoms.

The slopes for the pH 9.5, 11.0, and 12.2 solutions are
0.052, 0.046, and 0.046 respectively. These values are in-
termediate to the values in the more acidic and in the more
basic solutions. The values for the slopes of these curves
are probably too large for there is a continual decrease of
pH with increased current density. As mentioned earlier, this
gives a larger slope than expected.

Considered collectively, these curves are quite complex.
The overvoltage is a function not only of current density but
also of pH at the electrode (whether by change in acid con-
centration or by passage of current). The difference in reac-
tion mechanism in acidic and in basic solutions introduces
further complications.

Moreover, it was found that once the passive state of
iron is attained, it may be maintained by very low current
densities, i.e., the potential remains +0.7 displaced with
respect to that for the anodic dissolution of iron. Current
densities on the order of 0.1 uA/T.cm.^{2} were sufficient to
sustain oxygen evolution.

Decay of Anodic Polarization

When the potential of the iron electrode evolving oxygen
was allowed to decay under differing conditions, three types
of behavior were observed.
1. Section 1 of Figure 10 was obtained in neutral or basic
solution with anodic current densities sufficient for concen-
tration polarization. After decaying through (D), the arrests
(E) and (F) were observed before the potential stabilized at
(G) with hydrogen evolution.
2. Sections 4 and 5 of Figure 10 were obtained in acid solu-
tions. Unlike the first case, the potential immediately drops
to the arrest (F) and then passes to (G). The conditions that
exist at the surface of the iron should be identical to the
first case with the exception of the absence of concentration
polarization. This is shown by absence of arrest (E) in Sec-
tions 4 and 5.
3. In alkaline solutions with anodic current densities insuf-
ficient for concentration polarization effects, Section 3 of
Figure 10 was observed. The potential passes through only
one arrest (H') on the way to (G). The arrest (H') is 0.4 to
0.5 volt positive with respect to the arrest (F) obtained in
acid solution. Section 2 of Figure 10, also obtained in basic
solution, shows decay with small amounts of concentration po-
larization. This trace shows a mixture of arrests (E), (F),
and (H').

Sections 1 and 3 are identical to the traces of Figure 2.

Sections 1, 2, and 3 were taken with a solution of pH 11.6. The cathodic decay current density was 80 mA/A.cm.^{2}, and the anodic polarization current densities were 10, 0.5, and 0.1 mA/T.cm.^{2} for the three sections respectively. Sections 4 and 5 are traces at pH 2.5. The cathodic decay current density was the same as for Sections 1 - 3, and the anodic current densities were 1.0 and 0.01 mA/T.cm.^{2} respectively. The three types of behavior are called Cases 1, 2, and 3 and are discussed in that order.

All decay measurements were made with a recorder paper speed of 2"/second. Measurements indicated that this paper speed was constant and correct to better than 1 per cent.

Case 1

Decay in Alkaline and Neutral Solution with Large
Concentration Polarization Effects.

Experimental Results

The first step in all the decay traces was the instantaneous potential drop (D) shown in Figure 2. This is the decay of ohmic overvoltage. Its significance and utilization has been discussed in the oxygen overvoltage section.

Decay of concentration polarization (E):

Following (D), the potential arrest (E) Figure 2 was observed. Figure 10 is a more detailed composite trace of this and other potential-time behavior. In Section 1, the anodic current density of 10 mA/T.cm.^{2} is more than sufficient to cause the potential step of concentration polarization at a pH of 11.6. The upper sections of the curves of Figure 5 have anodic potentials between 1.2 and 1.4 volts for the two highest pH solutions. The potential of the arrest (E) begins at about 1.4 volts, decays slowly to about 1.2 volts, and then decays rapidly to (F). The arrest (E) was found to disappear for anodic current densities insufficient to cause concentration polarization at a given pH. Section 2 shows that a small amount of the arrest remains, and in Section 3, it has disappeared completely. Likewise, the arrest (E) was absent in the self-buffered acid solutions (Sections 4 and 5).

It was found that the length of existence of the arrest varied inversely with the bubbling rate, and this length varied inversely with the cathodic current density. The latter variation is illustrated in Figure 11. Here, the decay times are the average of four values for each cathodic decay current. The data are found to fit the equation

$$I = C/t - D \tag{11}$$

where I is the apparent cathodic current density, t is the time of existence of the arrest (E), and C, the slope and D, the intercept, are parameters.

For a given thickness of the diffusion layer (δ) and a given solution pH, there is a definite deficiency of hydroxyl ion in the diffusion layer. This deficiency can be formally represented as a charge separation Q. Cessation of the anodic current allows the destruction of this layer. It can be accomplished by diffusion, stirring, and/or passage of cathodic current. In Equation 11, C is the coulombic deficiency of hydroxyl ion per square centimeter in the diffusion layer. D should be considered as the "hydroxyl ion current density" of

Figure 11. Decay time versus the cathodic decay
current density for the break down of
concentration polarization.
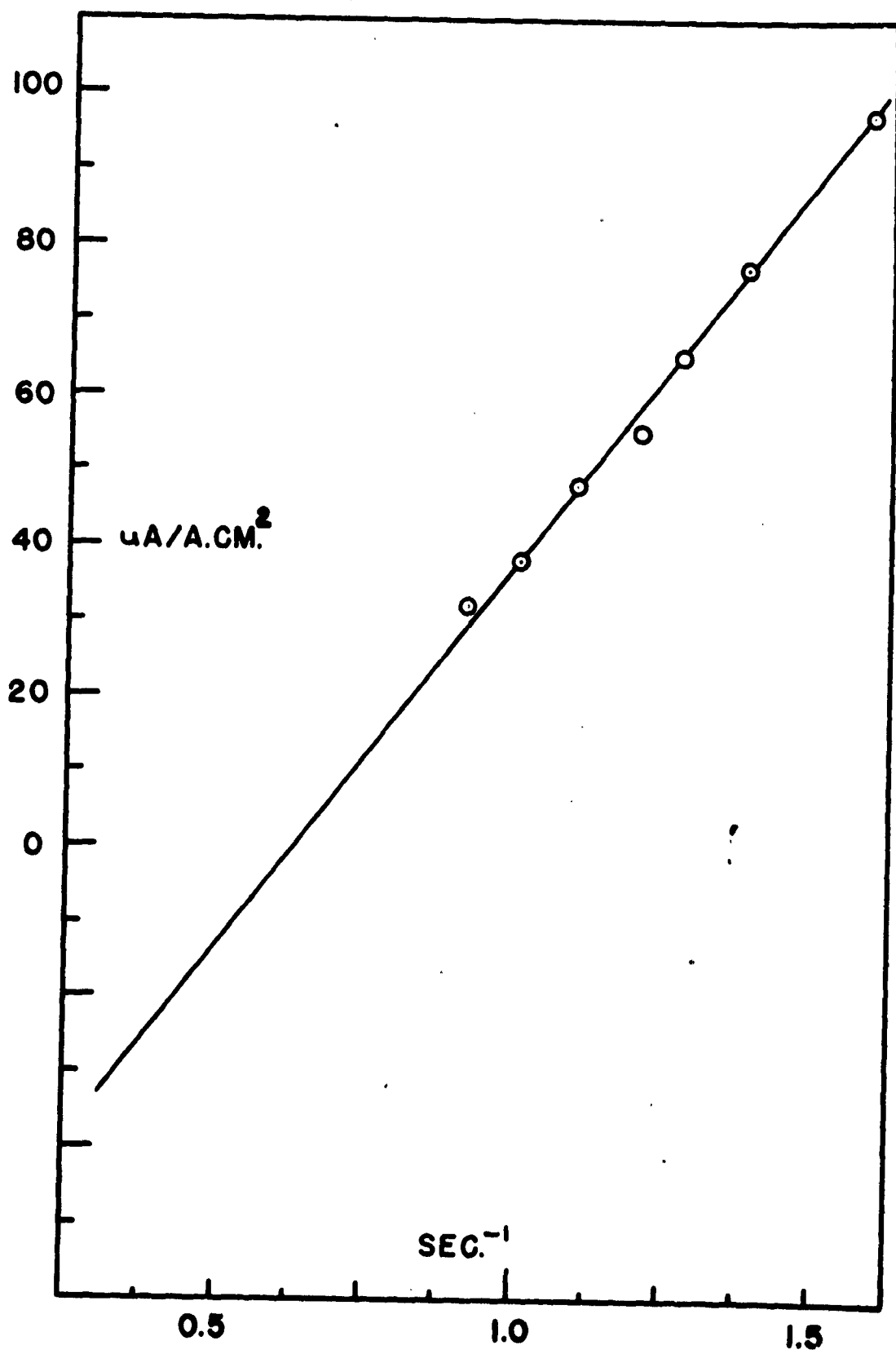
diffusion and stirring. Increasing the bubbling rate increases D and accounts for the decrease of t at constant I. Due to a relatively small decrease of δ with increased bubbling rates, there is also a slight secondary affect on C.

C can be calculated independently knowing the bulk concentration of hydroxyl ion, $(OH^-)_b$, the apparent area of the electrode, A, and the thickness of the diffusion layer, δ. The volume of the diffusion layer is

$$\delta A \times 10^{-3} \text{ liters} \tag{12}$$

With large amounts of concentration polarization, the (OH^-) at the electrode surface is zero when compared to $(OH^-)_b$, and the average concentration of hydroxyl ion in the diffusion layer may be taken as $(OH^-)_b/2$. The difference between this average and the bulk concentration is also $(OH^-)_b/2$. Assuming that the volume of the solution is large compared to the volume of the diffusion layer, the deficiency of hydroxyl ion in the diffusion layer is

$$\frac{\delta A(OH^-)_b \times 10^{-3}}{2} \tag{13}$$

and the deficiency in microcoulombs is

$$C = \frac{\delta A(OH^-)_b \times 10^{-3} \times F}{2} \tag{14}$$

where F is the Faraday.

For the data of Figure 11, A was 0.25 cm.^{2}, the pH was 11.6 $[(OH^-)_b = 7.35 \times 10^{-4}]$, δ was taken as the average of Table 3 $[3.4 \times 10^{-3}]$, and $F = 10^{-5}$. The theoretical deficiency is calculated to be

$$C = 31 \text{ microcoulombs}$$

The experimental slope is 10^4 microcoulombs/A.cm.^{2} For this electrode of area 0.25 cm.^{2},

$$C = 26 \text{ microcoulombs}$$

Decay of the protective covering (F):

After equalization of the hydroxyl ion concentration in the diffusion layer, the cathodic decay current removes any reducible chemical species adsorbed on the surface. This includes the hydroxyl radicals and lxygen atoms found to be adsorbed during the oxygen overvoltage experiments, as well as any protective covering such as ferric oxide. This process of reduction occurs at arrest (F). As mentioned in the introduction, the passive covering on iron is generally believed to be ferric oxide. All the following work indicates this is not the case for iron anodically passivated in Na$_2$SO$_4$.

Figure 12. Applied cathodic current density as a
function of reciprocal time for destruc-
tion of the protective layer.
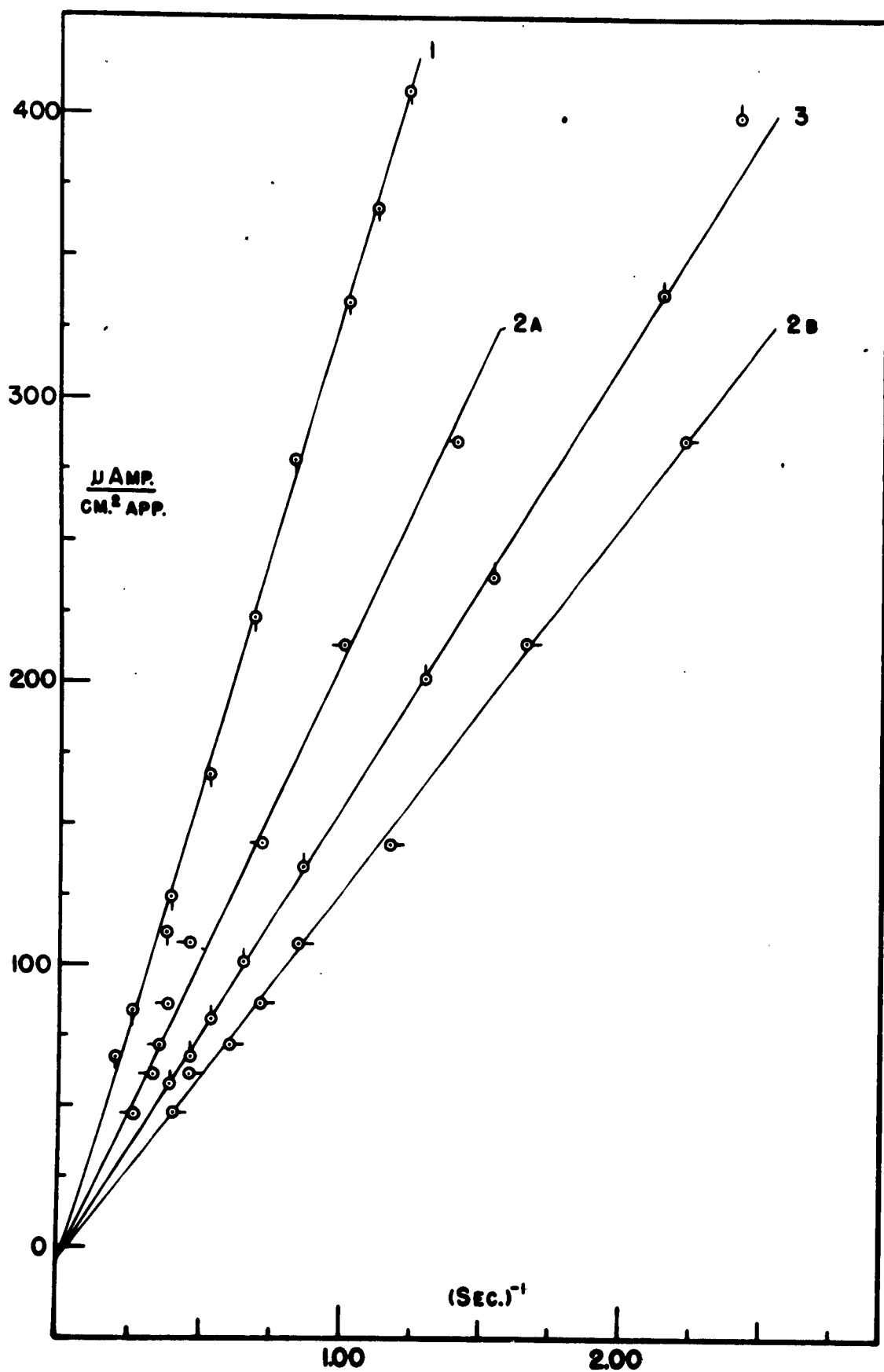
An examination of Section 1 of Figure 10 shows that after passing through (E) the potential falls rapidly to about +0.4 volt and then decreases slowly to about +0.05 volt. The potential then breaks off sharply and falls to (G). The break off potential signifying the end of arrest (F) varies randomly from 0.00 to +0.10 volts. This value is near the E^o for the oxygen electrode.

If a certain number of coulombs, cathodically passed, are required to remove the passive covering, then the length of arrest (F) should be inversely proportional to the applied cathodic current density. This type of relationship is identical with Equation 11 and is of the form

$$I = (e/t - f) \tag{15}$$

where I is the applied cathodic current density, and t is the time of existence. The slope e, and the y-intercept, f, are parameters which are constant for these experimental conditions.

Moreover, the overvoltage experiments revealed that the local cell current density was less than 0.1 uA/T.cm.^{2} Thus for applied cathodic current densities on the order of 50 to 500 uA/A.cm.^{2}, a plot of current density versus reciprocal time should extrapolate almost to the origin. Figure 12 shows several such sets of data. The small negative intercept is due primarily to the current drain for the recorder.

The coupons were alternately passivated for one minute and then forced to decay by cathodic polarization, the decay time being measured for various current densities. Each decay time shown is the average for four traces. The one minute passivation time was chosen arbitrarily, for experiments showed that the breakdown time was independent of the passivation time over the interval 0.25 to 180 minutes. The anodic current density prior to decay was 20.0 mA/A.cm.^{2}

Curve 2b was measured with no pre-roughening treatment. The slope is 130 uC/A.cm.^{2} The same coupon was then allowed to roughen for one hour at 20 mA/A.cm.^{2}, and the data of curve 2a were taken. The slope had increased to 212 uC/A.cm.^{2} The measurements of curve 1 were preceeded by the pre-roughening treatment used for the overvoltage measurements (20.0 mA/A.cm.^{2} for two hours). The slope of this curve is 335 uC/A.cm.^{2} With a 1/2 hour pre-roughening treatment, curve 3 showed that the slope was 160 uC/A.cm.^{2} Roughness factors of 7.7 and 2.8 are applicable to the measurements of curves 1 and 2b respectively. On the basis of the true areas, curves 1 and 2b give 43.5 and 46.5 uC/T.cm.^{2} The agreement of these values indicate that the increase of slope with increased roughening treatment arises from an increasing true surface area.

Determinations shown in Figure 12, as well as others, are

listed below.

Table 6

Curve	soln. pH	pre-roughening time	$uC/A.cm^2$	$uC/T.cm^2$
2b	6.8	0	130	46.5
3	11.0	1/2 hr.	160	-
2a	6.8	1 "	212	-
1	6.8	2 "	335	43.5
4	6.8	0 "	132	47.1
5	6.8	0 "	122	43.6
6	11.0	1/2 "	154	-
7	6.8	1/2 "	174	-
8	6.8	3/4 "	187	-
9	6.8	2 "	358	46.5

These results also indicate that the roughness factor increases with the length of anodic pretreatment. The average of slopes 1, 2b, 4, 5, and 9 is 45.4 $uC/T.cm^2$ This value can be used to calculate the roughness factors of other coupons given other pretreatments.

Next the arrest (F) was forced to decay under a small cathodic current. At various times during the disappearance of (F), small anodic charging currents were applied, and the number of coulombs necessary to regenerate oxygen evolution was determined. When the anodic charging current was applied, the potential increased linearly with time and then leveled off at the oxygen evolution potential consistent with the anodic current density. The dashed lines in Figure 10 show typical charging curves of this sort.

The charging curve results given here were taken following the measurements of curve 2a. The roughness factor was calculated by dividing the 212 $uC/A.cm^2$ by the 45.4 $uC/T.cm^2$ average. On this basis, the anodic charging current was about 20 $uA/T.cm^2$ The potential was forced to decay through step (F) by a cathodic current density of about 10 $uA/T.cm^2$, whereupon, the step lasted about 5 seconds. At various times during application of cathodic current, anodic charging current was substituted. The linear section of the charging curves was extrapolated to the resulting oxygen evolution potential (+1.2v.), and the time of charging to this potential was measured. The following table records the charging time, the cathodic decay time, and the number of microcoulombs necessary to restore oxygen evolution.

Table 7

Decay time elapsed	Charging time	Charging uC/T.cm.^{2}
1.9 sec.	0.35 sec.	7
3.1 "	0.55 "	11
4.2 "	0.68 "	14

Once the potential had decayed just beyond step (F), complete repassivation was required before oxygen evolution occurred again. That is to say, arrest (B), accompanied by dissolution of iron, needs to occur before oxygen evolution takes place. The number of coulombs necessary to regenerate oxygen evolution under these conditions was 10^3 times the values of the above table.

Discussion of Case 1

The results of the latter experiments indicate that the disappearance of arrest (F) is coincident with the removal of the protective covering on the passive iron surface. The coulombic requirements for charging the surface back to oxygen evolution increases with the time that the arrest (F) has decayed. On the order of 10 uC/T.cm.^{2} are required so long as the arrest (F) remains; however, once the potential has decayed past the arrest, the repassivation process must be accompanied by the dissolution of iron at arrest (B) of Figure 2.

The value of 45.4 uC/T.cm.^{2} for the removal of the protective covering corresponds to the transfer of 2.83×10^{14} electrons/T.cm.^{2} Assuming that the surface is covered with bulk oxide having a density of 5 g/cm.^{3} and that one electron is transferred for reduction of each iron ion in the oxide, the calculated thickness of the ferric oxide is 0.8Å. This is approximately ten times less than the unit cell dimensions of ferric oxide. If the oxide covering was of unit cell thickness, only ten per cent of the surface would be covered, and it would not be possible for the Fe_2O_3 to function as a protective physical barrier for the iron unless it is complete.

Bonhoeffer's[7] conclusion that the passive iron surface is covered with a monolayer of ferric oxide is apparently based on projected areas. Assuming a reasonable roughness factor of 3, the iron would be covered with one-third of a monolayer. As mentioned in the introduction, similar experiments on other passivatable metals lead to the conclusion that the surfaces of the metals are covered with a monolayer of the appropriate oxide.[8,9]

One square centimeter of iron surface contains 19.3×10^{14} iron atoms. Assuming that the surface is covered only with

hydroxyl radicals, which would require a one electron transfer per radical for production of hydroxyl ion, still only 15 per cent of the iron atoms have adsorbed radicals. However, Weiss[14] has shown that adsorbate-adsorbent interactions can produce potential fields extending over relatively large distances. If the species reduced during arrest (F) were adsorbed oxygen atoms, the surface coverage would be either 7.5 or 15 per cent depending on whether 1 or 2 electrons were transferred per atom during arrest (F). The overvoltage experiments in acid solutions indicate that there is adsorption primarily of hydroxyl radicals. A value of only 45 uC/T.cm.^{2} would dictate that there is no necessity for having chemical species other than the intermediates of oxygen evolution present on the surface (see later).

Case 2

Decay in Acid Solution

Experimental Results

The acidity of the solution at the surface of the electrode does not depend on the passage of current as in case 1, and the decay behavior is similar to case 1 with the exception of the absence of arrest (E) of concentration polarization. Within the limitations of the instrument, the decay trace of arrest (F) is identical in both cases. However, experiments in these acidic solutions brought out an entirely new phenomenon.
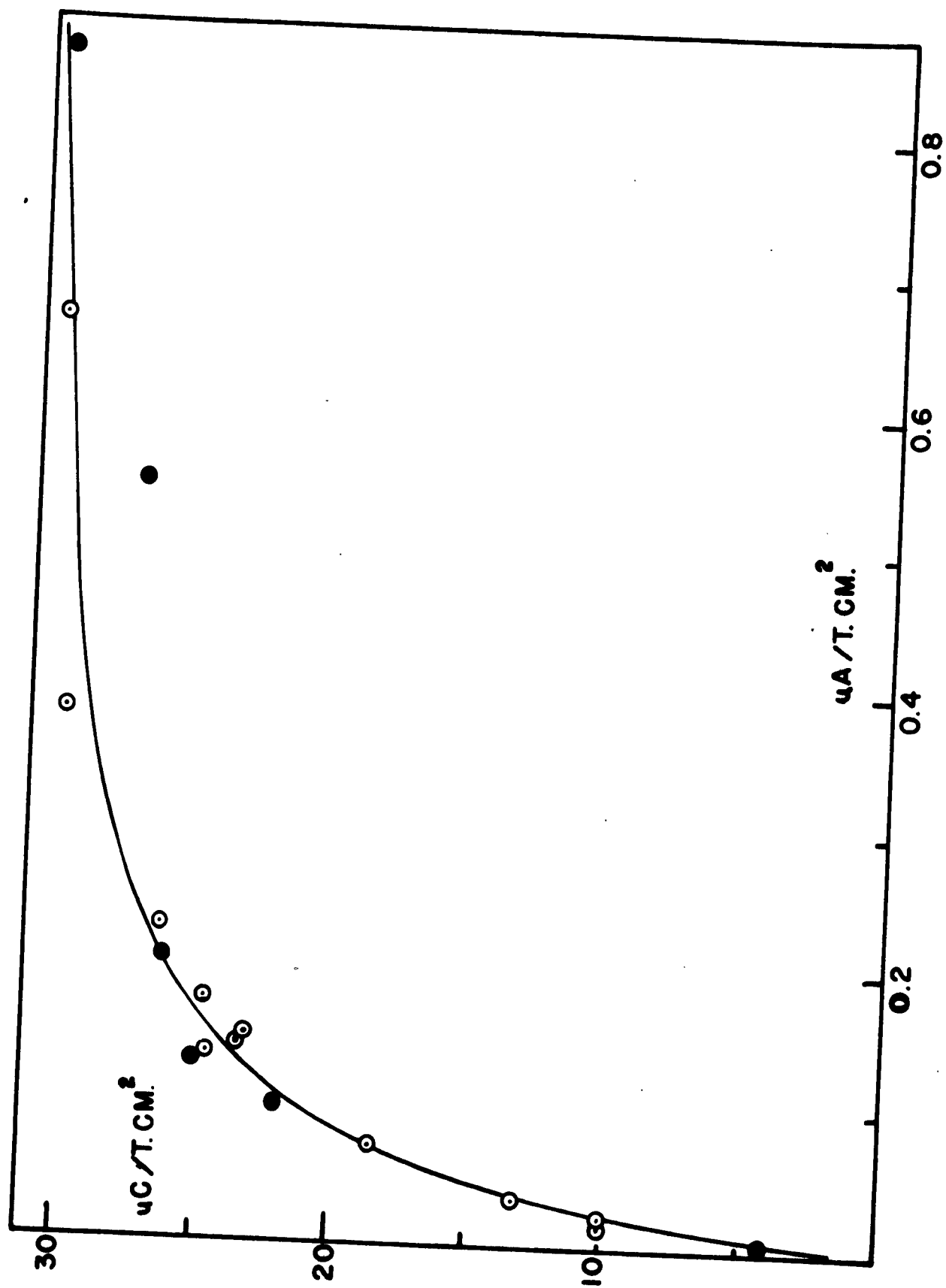
Previous decay traces had been taken with an anodic current density prior to decay of 20 mA/A.cm.^{2} In acid solutions, the current density can be reduced as low as desired without the appearance of arrest (H) of Figure 10 (obtained in alkaline solution with no concentration polarization) and withtou the disappearance of arrest (F). However, lowering the anodic current density prior to decay had the effect of reducing the surface coverage.
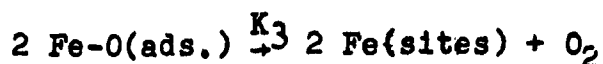
Arrest (F) was forced to decay from a previous anodic current density of 15.2 uA/T.cm.^{2} (there was no pre-roughening treatment), and the decay times were noted for a series of cathodic current densities. The slope of the data plotted, like that of Figure 12, was 36.8 uC/T.cm.^{2} At applied current densities of about 1 uA/T.cm.^{2}, the surface coverage started to fall off rapidly. Figure 13 shows the variation of surface coverage with the anodic current density going into the production of oxygen. Not all of the applied anodic current is used for liberation of oxygen. The recorder draws 0.8 uA/T.cm.^{2} These small currents become important when the applied anodic current is of the same order of magnitude. They do not affect the shape of the curve of Figure 13 but do affect the linear plot of the data. The recorder current is easily determined at any voltage by use of the calibrated resistor. The only method known for determining the local cell current density is to lower the anodic current density just to the point where the passive covering is no longer stable. At this point the anodic current density (corrected for the recorder current) is equal to the local cell current density. It was not considered necessary to have an independent evaluation of the local cell current density for the following work.

This decreased surface coverage behavior can be explained, assuming that arrest (F) corresponds to the removal of the intermediaries of oxygen evolution. The mechanism of oxygen evolution in pH 2.5 solution has been suggested as:

$$4\ H_2O + 4\ Fe(sites) - 4e \xrightarrow{K_1} 4\ Fe\text{-}OH(ads.) + 4\ H^+$$

Figure 13. Variation of surface coverage in uC/T.cm.^{2} with anodic current density going to the production of oxygen.

$$4 \text{ Fe-OH(ads.)} \xrightarrow{K_2} 2 \text{ Fe-O(ads.)} + 2 \text{ Fe(sites)} + 2H_2O$$

$$2 \text{ Fe-O(ads.)} \xrightarrow{K_3} 2 \text{ Fe(sites)} + O_2$$

Let the fraction of surface sites covered by hydroxyl radicals be X_1 and the fraction of sites covered by oxygen atoms be X_2. The rate of discharge of H_2O in the first step is directly proportional to the anodic current density, I, and the concentration of H_2O is constant. Consider the following rate equations:

Rate of formation of Fe-OH $= K_1 I^4 (1 - X_1 - X_2)^4$
Rate of disappearance of Fe-OH
Rate of Formation of Fe-O $= K_2(X_1)^4$
Rate of oxygen evolution $= K_3(X_2)^2$

Assuming there is no back reaction, the two steady state conditions for constant surface coverage are

$$K_2(X_1)^4 = K_1 I^4 (1-X_1-X_2)^4 \tag{16}$$

and

$$K_3(X_2)^2 = K_2(X_1)^4 \tag{17}$$

or

$$X_2 = \sqrt{K_2/K_3}\ (X_1)^2 \tag{17'}$$

Elimination of X_2 between Equations (16) and (17') gives

$$K_2(X_1)^4 = K_1 I^4 (1-X_1-\sqrt{K_2/K_3}X_1^2)^4 \tag{18}$$

The previous overvoltage measurements in acid solution showed that $K_3 > K_2$ and assuming that K_2 is negligible compared to K_3, equation (18) reduces to

$$(X_1) = \sqrt[4]{K_1/K_2}\ I(1-X_1)$$

and finally,

$$(X_1) = \frac{\sqrt[4]{K_1/K_2}\ I}{1 - \sqrt[4]{K_1/K_2}\ I}$$

The assumption that K_3 is much larger than K_2 implicitly assumes that X_1 is much greater than X_2 or that the surface is primarily covered with covered with hydroxyl radicals. This equation shows the same variation of surface coverage with anodic current as the Langmuir equation shows with pressure. It predicts that there is a finite maximum coverage, and that at small current densities the coverage decreases and eventually falls to zero. Since the fraction of the surface covered is directly proportional to the number of coulombs in arrest (F), a linear plot of I/X_1 versus X_1 can be used to

test the conformance of the data to equation 19.

The recorder·currents and the applied anodic currents were measured with the Rubicon potentiometer.· At the lower anodic current densities, 1/2 to 1 hour was required for the surface coverage to reach a steady value. The procedure used for the determination of surface coverages at the lower current densities was·to passivate ·in all cases at high current den-sities (20 mA/A.cm.^{2}) and to reduce the current density slowly to the value desired. When the surface coverage started falling off sharply, the measurements became very tedious. Small fluctuations in this region of current densities caused large variations in surface coverage. Moreover, in this region, the measured electrode potential also started to fall off sharply.

The coupons used in these measurements were given no pre-roughening treatment, and it was assumed that the small anodic current densities would not roughen them appreciably. Cathodic decay current used for all the measurements was 19.7 uA/T.cm.^{2}, and this includes the recorder current. The surface coverage is simply the product of the decay time and 19.7.

The local cell current was not determined. If it is not subtracted from the total applied current, a linear plot of the data of Figure 13 would show that the values of I/X$_1$ are too large at the smaller surface coverages. The local cell current was subtracted by trial and error until the plot was linearized. Figure 14 shows the result of this.

As mentioned earlier, when the surface coverage falls off, the electrode potential falls rapidly also. Figure 15 shows the potential change corresponding to each surface coverage at low current densities. The potential change is the dif-fernece between the oxygen evolution potential prior to decay and the break off potential of arrest (F), at which point the coverage has presumably fallen to zero. Uhlig[23] has inter-preted potential changes during the adsorption of inhibitors according to the following equation:

$$\Delta E = 4\pi n \mu / \chi \times 300 \qquad (20)$$

where n is the surface coverage in particles/T.cm.^{2}, and u is the dipole moment. There is quite a scattering of experimental points. The line drawn was calculated by the method of least squares. An evaluation of u from the slope indicates that the bonding electrons had shifted about 0.3% out from the surface of the iron. Moreover, extrapolation of ΔE to zero also shows that at this point, the surface coverage has fallen approximately to zero as is required by Equation (20)

Next, the anodic current density was reduced to the point where the surface coverage had fallen to a small value (about 4 uC/T.cm.^{2}). A small amount of potassium dichromate was then added to the solution. The potential immediately became about 0.1 volt more positive. After the potential had stabilized, it was allowed to decay under cathodic polarization. The

Figure 14. The linear plot for the variation of
surface coverage with anodic current
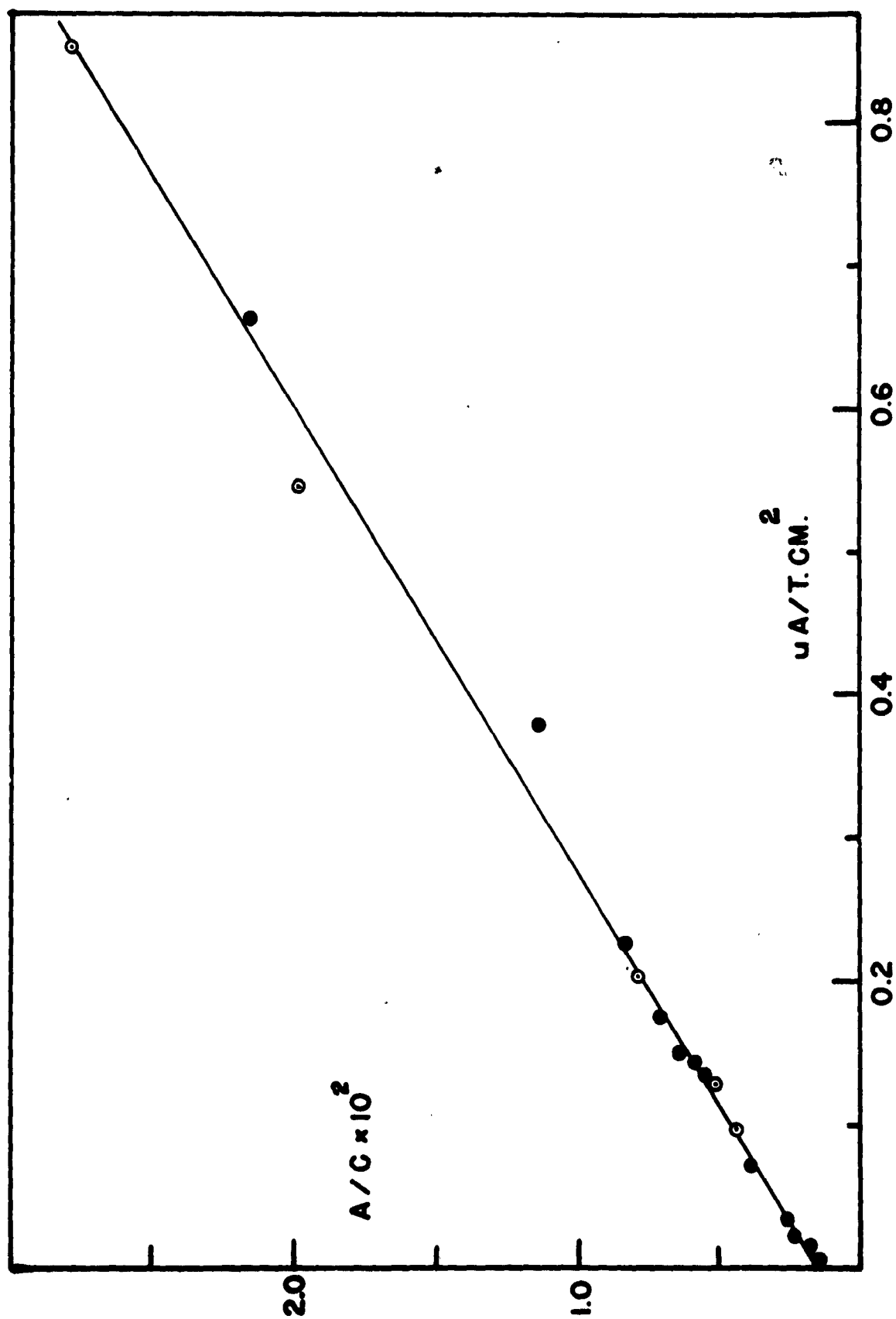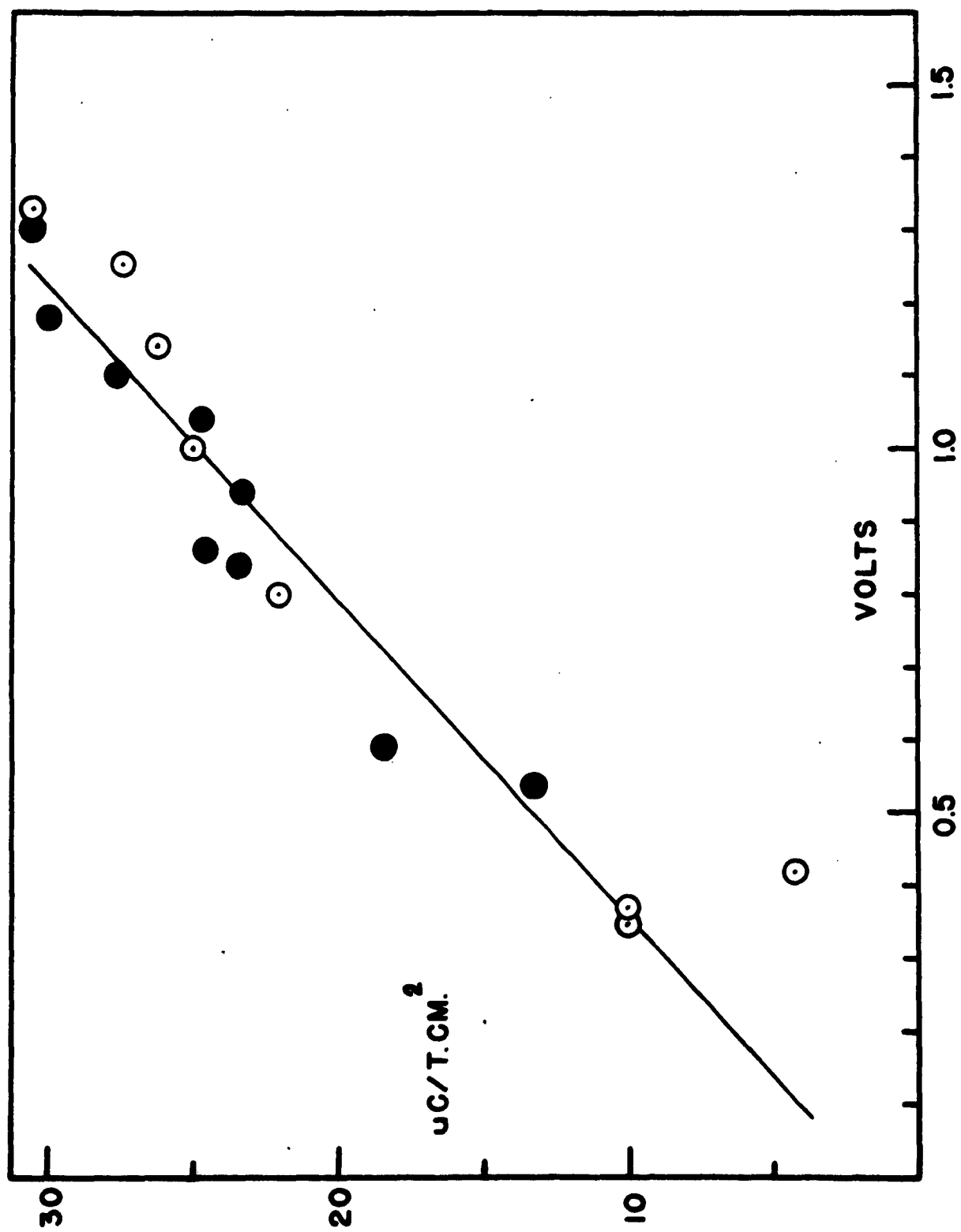density prior to decay.

44

Figure 15. Potential change corresponding to the
adsorption of the intermediaries of
oxygen evolution.

μC/T.CM.^{2}

VOLTS

30
20
10

0.5 1.0 1.5

surface coverage had increased to about. 30 uC/T.cm.^{2} With the
small suface coverage by hydroxyl radicals, there were many
sites on the surface available for adsorption of dichromate
ions. There may also be competitive adsorption between the
hydroxyl radicals already adsorbed and the dichromate ions.

Discussion of Case 2

All coupons were passivated at the same current density
and for measurement, the anodic current density prior to de-
cay was lowered to smaller values. It was found that the sur-
face coverage fell off as predicted by the theory developed
earlier. The theory necessitated a purely chemical path for
removal of the covering in order to explain the reduced cover-
age at low current densities.

The data of Figure 13 fit the concept that the protective
covering is hydroxyl radicals. The equation developed predicts
that the coverage is constant at large current densities and
drops off at small current densities. The assumptions under-
lying its derivation may not be completely valid; however, they
do not modify the general behavior — only the exact shape
of the theoretical curve. The dehydration of the hydroxyl
radicals and the combination of the resulting oxygen atoms is
a purely chemical path for the removal of the protective coating.

On the other hand, these data do not conform to Evans'
postulates for the nature of the covering. Evans[5,6] considers
that a passive iron surface is covered with ferric oxide and
has tried to show that this oxide can have the properties ne-
cessary for its protective character. He accounts for its
instability on the iron surface by its electrochemical reduc-
tion in the following cell:

$$Fe + Fe_2O_3 \rightarrow 3\ FeO$$
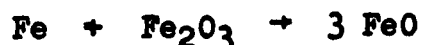
The ferrous oxide is soluble, and thus no longer protec-
tive. The ferric oxide that has been stripped from passive
iron surfaces was found to be insoluble, even in strong acid.
If the surface is covered with Fe_2O_3, then as long as the ano-
dic current density is greater than the local cell current
density for the dissolution of the Fe_2O_3, the surface coverage
should remain constant. It might be argued that the oxide is
thicker at large current densities; however, the coupons were
anodically polarized at the same current density prior to drop-
ping to small current densities where surface coverage dropped
off.

At the small current densities of the data of Figure 13,
the experimental curve levels off at 32 uC/T.cm.^{2} The rela-
tively slow increase from 32 to 45 uC/T.cm.^{2} for an anodic
current density is probably due to the reduction of oxygen

dissolved in solution. 32 uC/T.cm.^{2} corresponds to a 10 per cent coverage of iron atoms in the surface.

The applicability of Equation (20) to an electrode system with an external current flowing is open to question. The interpretation according to the application here would be that most of the overvoltage can be explained by a potential drop across the chemisorbed layer. On the basis of this equation, the calculated 0.3^o shift of the bonding electrons gives a negative space charge density on the surface of the iron electrode. This may explain the hydroxyl radicals' ability to inactivate an iron surface as pointed out in a similar case be Ershler.[3]

When the surface coverage by hydroxyl radicals is small, there should be many sites for specific adsorption of other species. Whether or not they adsorb depends on their individual adsorption characteristics as well as on the adsorption characteristics of the hydroxyl radicals. Apparently it is possible to adsorb dichromate ions when the surface coverage by hydroxyl radicals is small. This work does not show if dichromate ions can displace hydroxyl radicals already adsorbed. There are two possible explanations for the shift of potential when dichromate is added. First, the dichromate may be considered to be adsorbed on vacant sites, the new potential being characteristic of an iron surface covered primarily with dichromate ion just as there is a characteristic potential for the surface covered with the intermediate of oxygen evolution. Second, the dichromate may adsorb on different types of sites, and in some manner, lower the local cell current density so that more of the total applied anodic current density goes into the production of oxygen with resultant rise in electrode potential.

On the other hand, Evans[5] states that the protective action of dichromate is due to the formation of Cr_2O_3 on certain regions of the surface. The value of 30 uC/T.cm.^{2} allows for only a small amount of oxide and the same objections are valid as for the existence of ferric oxide on a passive surface.

Case 3

Decay of Overvoltage in Alkaline Solution with

No Concentration Overvoltage

Experimental Results

Section 3 of Figure 10 shows a typical decay curve when the solution adjacent to the electrode is alkaline. The anodic current density prior to decay was 0.10 mA/T.cm.^{2} At a pH of 11.6, this current density was insufficient to cause concentration polarization. On passing from oxygen to hydrogen evolution, there is a single arrest (H'), which is about 0.4 volt positive to arrest (F). The shapes of the two arrests are dissimilar. It might be argued that the two processes occurring at (F) and (H') are identical; that the difference in pH accounts for the difference in the two potentials. This cannot be the case. Careful adjustment of the anodic current density so that the solution adjacent to the electrode is only slightly alkaline shows a decay curve containing both arrests. This is illustrated in Section 2 of Figure 10. The anodic current density was 0.5 mA/T.cm.^{2} Thus the surface is covered with a mixture of components, each of which show a characteristic arrest on decay.

Using various cathodic decay currents, arrest (H') was forced to decay from the previous anodic current of 0.1 mA/T.cm.^{2} Figure 16 shows the variation of the breakdown time with the apparent cathodic current density. There was no pre-roughening of the surface, and the roughness factor was taken as 2.8. The slope of the curve is 110 uC/A.cm.^{2} or 39 uC/T.cm.^{2}

Discussion of Case 3

The existence of arrest (H') in alkaline solution only suggests that it is due to the desorption of hydroxyl ions. In acid solutions, the equilibrium concentration of adsorbed hydroxyl ions becomes negligible. Grahame[24] calculated that specific adsorption of hydroxyl ions on the positive side of the electrocapillary maximum of mercury gives a surface charge density of 15 to 25 uC/T.cm.^{2} The experimental value of only 39 uC/T.cm.^{2} is insufficient to account for covering by ferric oxide. In terms of a layer of adsorbed hydroxyl ions, the value compares favorably with Grahame's results. The adsorption of anions is specific in terms of both anion and adsorbent. Perfect agreement would not be expected between Grahame's values for mercury and this value for iron surfaces.

Figure 16. Breakdown time versus cathodic decay
current density for the protective
layer in alkaline solution.
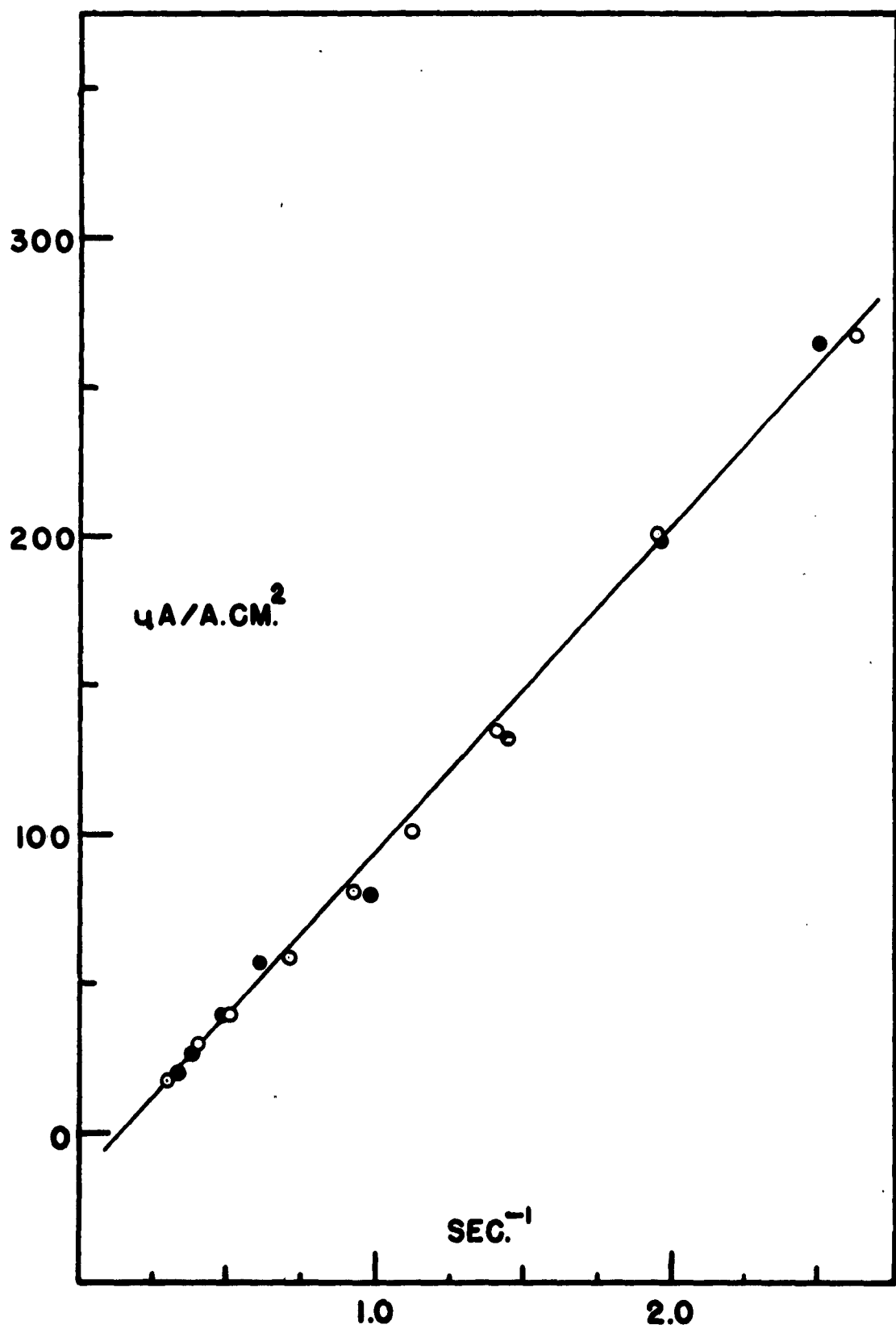
The passage of cathodic decay current in arrest (H') does not result in the transfer of electrons (chemical reduction). Just as a definite number of coulombs is passed to charge up a double layer without transfer of electrons, the 39 $uC/T.cm.^2$ Passed in arrest (H') is that required to discharge the double layer. (H') is probably the decay of only the inner Helmholtz layer of chemisorbed hydroxyl ions, and probably also includes a small amount of reduction of oxygen dissolved in solution.

General Discussion

Decay traces show that the passive surface of iron is protected by a chemical species equivalent to only 30 to 45 $uC/T.cm.^2$, and the data of Figure 13 show that considerably displaced potentials exist even though there is surface coverage corresponding to only 4 $uC/T.cm.^2$ The latter amount is equivalent to about 1 to 2 per cent coverage with oxygen atoms or ferric oxide of unit cell thickness. This low coverage requires that the layer have very intensive protective qualities. It is difficult to see how these qualities could be ascribed to an oxide of iron, especially when this oxide is stated to have the ordinary bulk properties.

On the other hand, a chemisorbed layer is more plausible in the light of the experimental data. Chemisorption bonds are as strong as chemical bonds, and there is no reason to believe that a chemisorbed monolayer should not be as protective as a layer of oxide of "true chemical compound." Moreover, a chemisorbed layer has the property of long range protection due to potential fields set up on the surface layer.

Many workers seem to have no difficulty in speaking of a monolayer of oxide. They feel that the properties of these monolayers are identical to the bulk properties. However, by its very essence, a bulk oxide must have three dimensional satisfaction of valence forces, which is not possible for a monolayer. Something akin to a monolayer of ferric oxide may be stabilized on the passive iron surface by chemisorption, but while serving in this protective manner, it surely would not have the properties of the bulk oxide.

It is possible that impurities remain on the surface following one or more passivation and activation cycles. However, these impurities can have little or no protective character. It has been assumed that any ferric oxide on the surface would be reduced upon cathodic decay prior to hydrogen evolution. The validity of this might be questioned. Evans and Berwick[25] have shown that blue tints of ferric oxide on iron are reduced during the decay of oxygen evolution, and there is no reason to believe that the reduction is not complete even to the thinnest remaining film. This, by itself, would indicate that once the potential passed through arrest (F) the surface is free of ferric oxide. Moreover, if patches of oxide remained on the surface following repeated passivation and activation cycles, the coupon would have been corroded unevenly. This was not found to be true. Although the repeated cycles increased the roughness factor, to about 8, the attack was quite general.

It is a fact that some metals such as aluminum do form protective oxides. This cannot be extrapolated to show that metals such as iron are protected by a similar type of covering.

It might be questioned whether or not the bulk oxide on aluminum is necessary for its protection and passivation. It is quite possible that the visible growth of the passive covering on aluminum is characteristic and not a necessity for passivation.

The existence of arrest (H') only in alkaline solution suggests that it is due to adsorption of hydroxyl ions, in addition to any adsorbed intermediates of oxygen evolution. In acid solution it is not so easy to determine the primarily adsorbed species. The decay curves offer little help, other than to rule out the existence of appreciable amounts of ferric oxide. Activation overvoltage measurements are the tools which furnish the details of the electrode reaction. The Tafel slope at pH 2.5 of 0.030 indicates that mechanism 1 of Table 5 is operative. This mechanism dictates that the surface be primarily covered with hydroxyl radicals.

Previously, there has been no discussion of the possible adsorption of ions from the acid solutions. Sulfate ions have been shown to adsorb on iron surfaces[26], and it is possible that some part of the 30 to 45 uC/T.cm.^{2} arises from desorption of the sulfate ions. In alkaline solution, arrest (H') is the only step observed. This shows the absence of sulfate ions which would desorb at arrest (F) on decay.

Mechanisms 6 and 7 of Table 5 have reaction steps that fit the data of alkaline solutions. The extensive coverage of the electrode with hydroxyl ions changes the mechanisms from that in acid solution. Instead of direct combination of oxygen atoms (these are probably generated in a manner identical to that for acid solution), there is the reaction between adsorbed hydroxyl ions and oxygen atoms to give oxygen molecules.

All the results presented here tend to show that while a normally active metal is in the passive state, its properties and behavior are identical to the truely inert metals such as platinum. There is little reason to say that this system is more complex and unmanageable than the inert metal systems.

REFERENCES

1. F. P. Bowden, Proc. Roy. Soc. (London) 125A, 446 (1929).

2. J. A. V. Butler and G. Armstrong, Ibid., 137A, 604 (1932)
   G. Armstrong, F. R. Himsworth, and J. A. V. Butler, Ibid.,
   143A, 89 (1933).

3. B. Ershler, Dic. Faraday Soc., 1, 269 (1947).

4. J. A. V. Butler and G. Drever, Trans. Faraday Soc. 32,
   427 (1936).

5. U. R. Evans, "Metallic Corrosion Passivity and Protection",
   Edward Arnold and Co., London, Second Edition, 1948.
   H. H. Uhlig (Editor), "Corrosion Handbook", John Wiley
   and Sons Inc., New York, 1951.

6. U. R. Evans, Ibid., pp. 31, 51-56.

7. K. F. Bonhoeffer, Zeitsch. Electrochem., 47, 147 (1941).

8. B. H. Roberts and W. J. Shutt, Trans. Faraday Soc., 34,
   1455 (1938).

9. A. Hickling and J. E. Spice, Ibid., 43, 762 (1947).
   S. E. S. ElWakked and A. Hickling, Ibid., 46, 820 (1950).
   A. Hickling and D. Taylor, Ibid., 44, 262 (1948).

10. M. G. Fontana, Corrosion, 3, 567 (1947). F. H. Beck,
    Eng. Exp. Sta. News, Ohio State University, December, 1947.

11. H. H. Uhlig, Trans. Electrochem. Soc., 85, 307 (1944);
    AIME T. P. No. 2243 (September, 1947).

12. T. Heumann, Zeitsch. Electrochem., 55, 287 (1951).

13. See reference 11 (H. H. Uhlig), p. 23.

14. P. B. Weisz, J. Chem. Physics, 21, 1531 (1953).

15. O. L. Willbanks, Thesis, The University of Texas, 1954.

16. M. J. Joncich, Dissertation, The University of Texas, 1953.

17. N. Komodromos, Thesis, The University of Texas, 1954.

18. J. H. Bartlett and L. Stephenson, J. Electrochem. Soc.,
    99, 504 (1952).

19. C. V. King, J. Electrochem. Soc., 102, 193, (1955).

20. J. O'M. Bokris, Am. Review of Phy. Chem., 5, 477 (1954).

21. A. Riuo, J. Llopis, and P. Gandia, Am. Real. Soc. esp.
     Fes. Quim., 46B, 279 (1950).

22. J. O'M. Bockris, "Modern Aspects of Electrochemistry",
     Academic Press Inc., New York, 1954, ch. 4.

23. H. H. Uhlig and A. Geary, J. Electrochem. Soc., 101,
     215 (1954).

24. D. C. Grahame, M. A. Poth, and J. I. Cummings, J. A. C. S.,
     74, 4422 (1952).

25. J. Chem. Soc., 1952, 3432.

26. N. Hackerman and S. J. Stephens, J. Phys. Chem., 58,
     904 (1954).

DISTRIBUTION LIST FOR TECHNICAL REPORTS

Contract Nonr-375(02)

Corrosion Research Laboratory

Director, Naval Research Laboratory
Washington 25, D. C.
Attn: Code 2500, Metallurgy Division
        Code 2020, Technical Library

Bureau of Aeronautics
Department of the Navy
Washington 25, D. C.
Attn: N. E. Promisel, AE-41   (2)
        Technical Library, TD-41

Commanding Officer
Naval Air Materiel Center
Naval Base Station
Philadelphia, Pennsylvania
Attn: Aeronautical Materials Lab.

Bureau of Ordnance
Department of the Navy
Washington 25, D. C.
Attn: Re Technical Library, AD3 (3)

Superintendent, Naval Gun Factory
Washington 25, D. C.
Attn: Metallurgical Lab., DE 713

Commanding Officer
U. S. Naval Ordnance Laboratory
White Oak, Maryland

Commanding Officer
U. S. Naval Ordnance Test Station
Inyokern, California

Bureau of Ships
Department of the Navy
Washington 25, D. C.
Attn: Code 343   (2)
        Code 337L, Tech. Library (1)
        Code 347   (1)

Wright Air Development Center
Wright-Patterson Air Force Base, Ohio
Attn: Materials Laboratory   (1)
        Flight Research Laboratory (1)
            (J. B. Johnson)

Bureau of Yards and Docks
Department of the Navy
Washington 25, D. C.
Attn: Research and Standards Division

Post Graduate School
U. S. Naval Academy
Monterey, California
Attn: Department of Metallurgy

Office of the Chief of Ordnance
Research and Development Service
Department of the Army
Washington 25, D. C.
Attn: ORDTB   (3)

Commanding Officer
Watertown Arsenal
Watertown, Massachusetts
Attn: Laboratory Division

Commanding Officer
Frankford Arsenal
Frankford, Pennsylvania
Attn: Laboratory Division

Office of the Chief of Engineers
Department of the Army
Washington 25, D. C.
Attn: Research & Development Branch

U. S. Air Forces
Research and Development Division
The Pentagon
Washington 25, D. C.

Chief of Staff, U. S. Army
The Pentagon
Washington 25, D. C.
Attn: Director of Research and
            Development

U. S. Naval Engineering Experiment
    Station
Annapolis, Maryland
Attn: Metals Laboratory

- 2 -

Director, Materials Laboratory
Building 291
New York Naval Shipyard
Brooklyn 1, New York
Attn: Code 907

Chief of Naval Research
Department of the Navy
Washington 25, D. C.
Attn: Code 423   (2)

Director
Office of Naval Research
Branch Office
346 Broadway
New York 13, New York

Director
Office of Naval Research
Branch Office
844 North Rush Street
Chicago 11, Illinois   (2)

Director
Office of Naval Research
Branch Office
1000 Geary Street
San Francisco 9, California

Director
Office of Naval Research
Branch Office
1030 East Green Street
Pasadena 1, California

Assistant Naval Attache for Research
Office of Naval Research
Branch Office
Navy 100
c/o Fleet Post Office
New York, New York   (2)

Carbide and Carbon Chemicals Division
Plant Records Department
Central Files (K-25)
Post Office Box P
Oak Ridge, Tennessee

Carbide and Carbon Chemicals Division
Central Reports and Information
   Office (Y-12)
Post Office Box P
Oak Ridge, Tennessee

Director
Naval Research Laboratory
Washington 25, D. C.
Attn: Technical Information Center (6)

Commanding Officer
Office of Ordnance Research
Duke University
Durham, North Carolina
Attn: Metallurgy Division

Atomic Energy Commission
Division of Research
Metallurgical Branch
Washington 25, D. C.

National Bureau of Standards
Washington 25, D. C.
Attn: Physical Metallurgy Division

National Advisory Committee
   for Aeronautics
1724 F. Street, N. W.
Washington 25, D. C.

Research & Development Board
The Pentagon
Washington 25, D. C.
Attn: N. C. Fick

Argonne National Laboratory
P. O. Box 5207
Chicago 80, Illinois
Attn: Dr. Hoylande D. Young

U. S. Atomic Energy Commission
1901 Constitution Avenue, N. W.
Washington 25, D. C.
Attn: B. M. Fry

Brookhaven National Laboratory
Information and Publication Division
Documents Section
Upton, New York
Attn: Miss Mary E. Waisman

Armed Services Technical Information
   Agency
Documents Service Center
Knott Building
Dayton 2, Ohio   (5)

- 3 -

General Electric Company
Technical Services Division
Technical Information Group
Post Office Box 100
Richland, Washington
Attn: Miss M. G. Freidank

Iowa State College
Post Office Box 14A, Station A
Ames, Iowa
Attn: Dr. F. H. Spedding

Knolls Atomic Power Laboratory
Post Office Box 1072
Schenectady, New York
Attn: Document Librarian

Los Alamos Scientific Laboratory
Post Office Box 1633
Los Alamos, New Mexico
Attn: Document Custodian

U. S. Atomic Energy Commission
New York Operations Office
Post Office Box 30, Ansonia Station
New York 23, New York
Attn: Division of Tech Information
        and Declassification Service

Oak Ridge National Laboratory
Post Office Bcx P
Oak Ridge, Tennessee
Attn: Central Files

Sandia Corporation
Sandia Base
Classified Document Division
Albuquerque, New Mexico
Attn: Mr. Dale M. Evans

U. S. Atomic Energy Commission
Library Branch, Technical Information
    Service, ORE
Post Office Box E
Oak Ridge, Tennessee

Westinghouse Electric Corporation
Atomic Power Division
Post Office Box 1468
Pittsburgh 30, Pennsylvania
Attn: Librarian

University of California
Radiation Laboratory
Information Division
Room 128, Building 50
Berkeley, California
Attn: Dr. R. K. Wakerling

Professor R. F. Mehl
Metals Research Laboratory
Carnegie Institute of Technology
Pittsburgh, Pennsylvania

Massachusetts Institute of Technology
Department of Metallurgy
Cambridge 39, Massachusetts
Attn: Prof. H. H. Uhlig

Professor P. Van Rysselberghe
University of Oregon
Eugene, Oregon

Professor A. T. Gwathmey
University of Virginia
Department of Chemistry
Charlottesville, Virginia

Professor P. Delahay
Louisiana State University
Baton Rouge, Louisiana

Professor W. D. Robertson
Department of Metallurgy
Yale University
New Haven, Connecticut

Professor H. J. Yearian
Physics Department
Purdue University
Lafayette, Indiana

Office of Naval Research
Navy Department
Washington 25, D. C.
Attn: Chemistry Branch, Code 425

Deterioration Prevention Center
2101 Constitution Avenue
Washington, D. C.
Attn: D. G. Greathouse.

Professor Carl Borgmann
University of Nebraska
Lincoln, Nebraska